Hindawi
International Journal of Energy Research
Volume 2024, Article ID 5724653, 31 pages
https://doi.org/10.1155/2024/5724653

Research Article

Operation Scheduling of Distribution Network with Photovoltaic/Wind/Battery Multi-Microgrids and Reconfiguration considering Reliability and Self-Healing

Alireza Kalantari and Hamid Lesani

School of Electrical and Computer Engineering, College of Engineering, University of Tehran, Tehran, Iran

Correspondence should be addressed to Hamid Lesani; lesani@ut.ac.ir

Received 7 December 2023; Revised 29 February 2024; Accepted 22 March 2024; Published 17 May 2024

Academic Editor: Subhashree Choudhury

In this paper, a new simultaneous framework of distribution network operation is proposed based on the scheduling of photovoltaic/wind/battery multi-microgrids with network reconfiguration considering self-healing. The objective function is considered to minimize the energy losses, and multi-microgrids cost and improve the reliability indices including minimization of energy not-supplied (ENS) and minimizing system average interruption duration (SAIDI) and system average interruption frequency (SAIFI) indices. The optimization variables are defined as the situation of the distribution network switches to find the network's optimal configuration with the installation location and size of renewable resources and battery energy storage during 24 hours. An improved beluga whale optimization (IBWO) based on a nonlinearly diminishing inertia weight (NDIW) approach is used to find the optimal variable set of the problem. The recommended methodology is implemented on 33-bus and real 59-bus distribution networks. The results demonstrated that by obtaining an optimal state of the network switches in the event of a fault, as well as the optimal scheduling of the two microgrids, the energy losses have decreased and the reliability indices have improved. The outcomes of the proposed methodology based on the hybrid multi-microgrid allocation and network reconfiguration are stated that the losses, ENS, SAIDI, and SAIFI are reduced by 66.39%, 54.00%, 50.24%, and 33.61%, respectively, for 33-bus network and are declined by 65.29%, 57.44%, 48.63%, and 62.33%, respectively, for the real 59-bus Ahvaz network in comparison with the base network. The obtained results illustrated that in the condition of the network line outage, by simultaneously implementing the reconfiguration with the change of network switches and the optimal allocation and scheduling of HMGs in the network, self-healing is provided to prevent a significant weakening of the network performance so that the resilience is improved in addition to minimizing the energy losses and the cost of HMG energy injection compared to the base network. The findings revealed that the objectives including losses, ENS, SAIFI, and SAIDI are increased by 78.29%, 33.00%, 83.33%, and 35.11%, respectively, due to outage of line 22 of the 33-bus network and these objectives are increased by 52.32%, 10.30%, 32.29%, and 79.66%, respectively, due to outage of line 12 of the 59-bus network compared with not considering the line outage. Moreover, the superior capability of the recommended NDIW-based IBWO has been confirmed in comparison with the well-known particle swarm optimizer (PSO) and ant lion optimizer (ALO) in solving the problem to achieve better objective value.

1. Introduction

1.1. Motivation and Backgrounds. The improvement of distribution network reliability is one of the key objectives in today's operational planning of distribution networks. The duty of distribution networks in meeting subscriber needs is growing increasingly important, and other traditional distribution networks are no longer responsive to subscriber needs due to the increasing consumption of electrical energy, changing customer behavior and demographics, and expanding subscriber numbers [1]. Although distribution networks are responsible for the bulk of consumer outages, many subscriber outages are also caused by distribution network problems, which can lead to component failures, line

outages, and subscription outages [2]. Due to a lack of automation and reliance on manual processes for conventional distribution networks, there are more subscribers and longer outages as a result of a variety of factors and lax monitoring. As a result, the network's level of reliability declines [3, 4]. Also, the concern over climatic and environmental alterations, as well as the rise in emissions of greenhouse gases, has prompted researchers to consider alternatives to conventional production sources for power systems that utilize fossil fuels. As a result, renewable energy sources play a significant role in smart distribution networks. Network operators have become interested in microgrids because they can improve the reliability of the network by including renewable energy sources and storage components [5]. On the other hand, via microgrids based on energy from renewable sources, it is possible to increase self-healing [6] and reliability in the event of a mistake or outage of network lines based on the automation of the distribution network based on reconfiguration, by changing the state of the network switches.

1.2. Literature Review and Research Gap. Numerous researches have been done in the area of operating distribution networks according to the planning of renewable energy sources, particularly hybrid energy microgrids (HMGs). To minimize costs, simultaneous installation of remote control switches and manual control is a challenge that is addressed in [7]. To solve this problem, reliability indices and HMGs are utilized in this study. To assess the kind and condition of automation technology concurrently, as well as to reduce costs and boost reliability metrics, integer linear programming is provided in [8]. HMG and its impact on enhancing reliability are not taken into account in this study. To cut costs and boost reliability indices, self-healing has been improved by employing electric vehicle parking planning ability in Ref. [9]. The effectiveness of reconfiguring based on network switches to increase reliability has not been assessed in this research. In [10], the evolutionary algorithm is used to develop the best option for distributed generation allocation to increase reliability in a distribution network. The use of HMGs and network reconfiguration was not attempted in this study to increase resilience. In [11], the optimum functioning of electric vehicles and energy sources is implemented in a smart network with the capability to inject electricity into the grid to minimize the cost of bought power from the primary electrical system and the penalty of weakening resilience. It is discovered where to install and how big to make these components so as to maximize profitability. In [12], an advantageous approach for allocating electric parking lots to enhance network dependability and cost minimization is performed in distribution networks. According to various degrees of vehicle adoption and resilience, Landi et al. [13] present distributing the electric parking lots for minimizing operational costs, the cost of charging and discharging vehicles, and the cost of obtaining electricity from the main grid. The impact of reconfiguration and energy multi-HMGs on reliability measures is not assessed in [11–13]. In [14], the augmented genetic optimization technique is examined for the static reconfiguration of balanced networks to reduce losses and increase resilience. In [15], a combination of the exchange market algorithm and the wild goat algorithm is presented for dynamic multi-criterion reconfiguration of balanced distribution networks to identify the best network configuration for reliability improvement and loss minimization. The impact of energy multi-HMGs on reliability metrics is not examined in [14, 15]. In [16], it allocates the PVs and WTs in a balanced network using a hybrid teaching-learning-gray wolf optimizer method to reduce losses and improve dependability. In [17], the bat algorithm is used to schedule wind and solar resources while taking resilience. According to [18], network reconfiguration and PV and WT allocation in a balanced network are recommended for lowering losses and voltage variations and enhancing voltage stability and dependability with the use of a moth flame optimizer. The impact of reconfiguration on reliability metrics is not assessed in [17, 18]. In [19], a method for dynamic reconfiguration is presented that minimizes losses and voltage variations to increase network resilience. Using particle swarm optimization, Sannigrahi et al. [20] develops an allocation of integrated energy resources with regulated network reconfiguration to increase voltage stability and resilience, lower pollution, and maximize net savings. The improvement in self-healing under fault incidence in the network is not assessed in this study. A line hardening and DG setup technique is provided in [21] with the goal of improving distribution network reliability while reducing load reduction across the board using updated column and restriction-producing algorithms. In [22], a mixed-integer programming model is used for carrying out restoration scheduling for grid-enabled electric vehicles in the distribution network in an effort to reduce the overall cost of system functionality loss. To reduce the investment cost, Hou et al. [23] proposes a distribution network reliability upgrade that is structured as a mixed-integer linear programming model with the installation of DGs, the allocation of mobile backup generators, and the deployment of switches. In [24], the resilient distribution network operation is evaluated in the presence of smart parking lots and renewable energy sources. Demand response applications, battery energy storage devices, and standby diesel generators are recommended to enhance the network's resiliency. In [25], a mixed-integer linear programming framework is developed for the best placement of backup DGs and sectionalizing switches to increase reliability in emergency situations while taking into account energy unnerved. In [26], the distribution network's robustness is improved to both the direct and indirect effects of strong winds by taking into account the wide range of batteries. The objective function of the reduced vital loads achieves the optimal quantity of power and energy for batteries for different technologies. In [27], an operational structure that utilizes mobile energy hubs and the shortest path algorithm is presented to enhance distribution network resilience. To maximize the restoration of important loads, an efficient management solution is also offered to improve the performance of electrical distribution networks. The impact of energy multi-HMGs, network reconfiguration, and self-healing is not examined or assessed in [23–27] for reliability metrics. The literature review summary is presented in Table 1.

Table 1: The literature review summary.

Ref.	Reconfiguration	HMG			Objective function			Self-healing	Improved Solver
		PV	WT	Battery	Loss	Reliability	Cost		
[7]	Yes	No	No	No	Yes	Yes	Yes	No	No
[8]	Yes	No	No	No	Yes	Yes	No	No	No
[9]	No	No	No	No	No	Yes	No	Yes	No
[10]	No	Yes	No	No	Yes	Yes	Yes	No	No
[11]	No	Yes	Yes	Yes	No	No	Yes	No	No
[12]	No	Yes	Yes	Yes	No	No	Yes	No	No
[13]	No	No	No	Yes	Yes	No	Yes	No	No
[14]	Yes	No	No	No	Yes	Yes	No	No	No
[15]	Yes	No	No	No	Yes	Yes	No	No	No
[16]	No	Yes	Yes	No	Yes	Yes	No	No	Yes
[17]	No	Yes	Yes	No	Yes	Yes	Yes	No	No
[18]	Yes	Yes	Yes	No	Yes	Yes	No	No	No
[19]	Yes	No	No	No	Yes	Yes	No	No	No
[20]	Yes	Yes	Yes	No	Yes	Yes	No	No	Yes
[21]	No	Yes	No	No	Yes	Yes	No	No	No
[22]	No	No	No	Yes	Yes	No	Yes	No	No
[23]	No	Yes	No	No	Yes	Yes	Yes	No	No
[24]	No	Yes	Yes	No	Yes	Yes	Yes	No	No
[25]	Yes	Yes	No	No	Yes	Yes	No	No	No
[26]	No	No	Yes	No	No	No	Yes	No	No
[27]	No	Yes	No	No	Yes	No	Yes	No	Yes
This paper	Yes	Yes	Yes	Yes	Yes	Yes	Yes	Yes	Yes

Following an assessment of the literature, the following research gaps are listed:

(i) Reviewing the studies revealed that the utilization of electric parking lots, distributed production resources, renewable energy sources, network reconfiguration by identifying the open and closed switches of the network, and the best allocation of resources have all been done in order to improve the self-healing of the network and increase resilience. The impact of choosing the installation site and the ideal capacity of renewable resources on enhancing the network's dependability has been examined in some research. Studies have revealed that simultaneous employment of integrated approaches to increase reliability and self-healing improvement is less common

(ii) The issue of enhancing self-healing brought on by fault-related conditions by applying network automation based on reconfiguration as well as multi-HMGs based on storage element has not been addressed in the studies that have been undertaken. The absence of a multi-objective planning operation to achieve the best configuration of the network, locate the placement of the energy HMGs within the network, and plan their energy distribution over the study horizon is consequently simultaneously felt

(iii) The operation of renewable energy HMGs simultaneously with storage components in distribution networks and network reconfiguration presents a number of difficulties, among them the most important of which is figuring out where to place HMGs in the network, where to plan for resources and storage, and how to best configure the network. If these factors are wrongly determined, the performance of the network will suffer. However, due to their early convergence problems, particularly in the case of multi-HMGs, conventional approaches are unable to overcome this problem. On the other hand, in order to optimally determine the open and closed switches of the network, the best location for installation, and the capacity of the energy multi-HMG components during the study period, it is essential to set up a metaheuristic method with high exploration and exploitation power

1.3. Contributions. According to the existing research gaps, the contributions of this research are presented as follows:

(i) This study presents the operation of 33-bus and a real 59-bus distribution network allocation and scheduling using the multi-HMG structure of energy with network reconfiguration to improve reliability while taking self-healing into account

(ii) The reliability of the network has been increased based on the scheduling of multi-microgrids, including

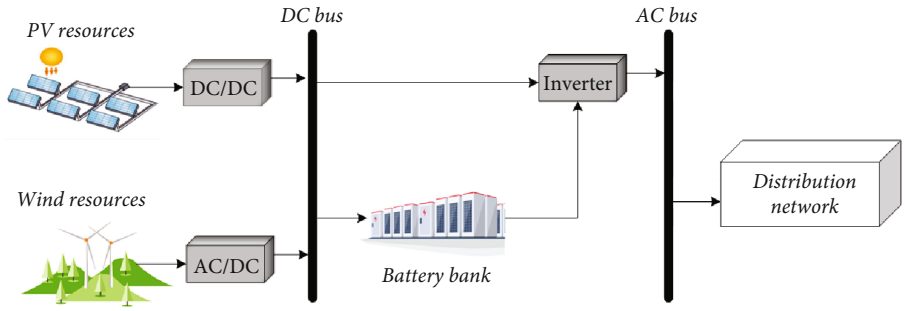

Figure 1: Schematic of the HMG system connected to the radial distribution network.

photovoltaic and wind energy sources integrated with battery storage, and simultaneously adjusting the state of the network switches in the event of a fault and injecting its planned power into the distribution network

(iii) A multi-objective function is defined, which includes minimizing energy loss; improving reliability indices like ENS (energy not-supplied), SAIDI (system average interruption duration index), and SAIFI (system average interruption frequency index); and minimizing the cost of multiple HMGs

(iv) The optimal state of network switches or optimal network configuration, as well as the ideal location for installing multi-HMGs and their optimal scheduling, has all been found via an improved metaheuristic algorithm. The conventional beluga whale optimization (BWO) is inspired according to behaviors of pair swim, prey, and whale fall [28]. In this paper, conventional BWO is improved based on the nonlinearly diminishing inertia weight approach [29] to overcome the premature convergence and the improved version named IBWO

1.4. Paper Structure. The HMG component modeling is given in Section 2. The problem objective function and the constraints are formulated in Section 3. The proposed optimization approach and its steps for problem solving are presented in Section 4. In Section 5, simulation results in different scenarios are given. Finally, the outcomes of the study are concluded in Section 6.

2. HMG System Modeling

An HMG made up of solar (PV) energy sources, wind turbine (WT) energy sources, and battery (BA) storage is taken into consideration in this study according to Figure 1. The DC/AC converter is the last piece of apparatus before the load in the HMG system, and its job is to convert DC power to AC power. Battery storage is used in HMG to equalize power oscillations and provide continuous power with the necessary level of dependability to the load on the distribution network.

2.1. PV Model. The PV array's power output is determined using its surface temperature, rated power, and radiation intensity as follows [30, 31].

$$P_{\mathrm{PV}} = P_{\mathrm{PV-Rated}} \times \frac{\partial}{\partial_{\mathrm{Ref}}} \left(1 + \gamma_{\mathrm{TC}}(\mathrm{TEM}_C - \mathrm{TEM}_R)\right),$$
$$P_{\mathrm{PV}}^T = n_{\mathrm{PV}} \times P_{\mathrm{PV}}, \tag{1}$$

where ∂ is the radiation perpendicular to the surface of the array ($\mathrm{W/m^2}$), n_{PV} is the number of panels, $P_{\mathrm{PV-Rated}}$ is the rated power of each PV panel, ∂_{Ref} is the amount of standard radiation (i.e., $1000\,\mathrm{W/m^2}$), γ_{TC} is the temperature coefficient of the PV panel (-0.0037 per degree Celsius), TEM_R is the temperature of the PV in the reference condition, and TEM_C represents the temperature of the cell.

2.2. WT Model. This nonlinear relationship between the power WT extracts and changes in wind speed is shown in the following charts [30, 31]:

$$P_{\mathrm{WT}} = \begin{cases} 0 & \mathrm{WS} \le \mathrm{WS}_{\mathrm{Cut-in}} \quad \text{and} \quad \mathrm{WS} \ge \mathrm{WS}_{\mathrm{Cut-out}}, \\ P_{\mathrm{WT-Rated}} \times \left(\dfrac{\mathrm{WS} - \mathrm{WS}_{\mathrm{Cut-in}}}{\mathrm{WS}_{\mathrm{Rated}} - \mathrm{WS}_{\mathrm{Cut-in}}}\right) & \mathrm{WS}_{\mathrm{Cut-in}} \le \mathrm{WS} \le \mathrm{WS}_{\mathrm{Rated}}, \\ P_{\mathrm{WT-Rated}} & \mathrm{WS}_{\mathrm{Rated}} \le \mathrm{WS} \le \mathrm{WS}_{\mathrm{Cut-out}}, \end{cases}$$
$$P_{\mathrm{WT}}^T = n_{\mathrm{WT}} \times P_{\mathrm{WT}}, \tag{2}$$

where P_{WT} is the output power of WT, the rated power of each turbine, v is the wind speed. WS_{Cut-in}, $WS_{Cut-out}$, and WS_{Rated} are the cut-in speed, cut-out speed, and rated wind speed, and n_{WT} indicate the number of WTs.

2.3. Battery Charge and Discharge Models

(i) *Charging model*: the battery is put into a charging state when $P_{PV}^{T}(t) + P_{WT}^{T}(t)/\gamma_{INV} > P_{NET}(t)$, and the extra electricity of the HMG is supplied into it. The energy content of the batteries at time t is computed in the following way [30, 31]:

$$E_{BA}(t) = (1-\varpi) \times E_{BA}(t-1) + \left[\left(P_{PV}^{T}(t) + P_{WT}^{T}(t)\right) - \frac{P_{NET}(t)}{\gamma_{INV}}\right] \times \Delta t \times \gamma_{BA}, \tag{3}$$

where $E_{BA}(t)$ and $E_{BA}(t-1)$ are the battery energy values at hours t and $t-1$, $P_{NET}(t)$ is the load demand at time t, γ_{INV} is the inverter efficiency, ϖ is self-discharge, Δt is time steps (1 hour), and γ_{BA} refers to the battery charging yield.

(ii) *Discharge model*: the batteries are in discharge mode when $P_{PV}^{T}(t) + P_{WT}^{T}(t)/\gamma_{INV} < P_{NET}(t)$, to make up for the network load power deficiency (P_{NET}), and the batteries can make up for an HMG lack of power. The energy of the batteries at time t is computed as follows [30, 31]:

$$E_{BA}(t) = (1-\varpi) \times E_{BA}(t-1) - \left[\frac{P_{NET}(t)}{\gamma_{INV}} - \left(P_{PV}^{T}(t) + P_{WT}^{T}(t)\right)\right] \times \Delta t. \tag{4}$$

2.4. Inverter Model. The transferred power from the inverter to the load demand is computed by

$$P_{Inv-Load} = (P_{BA-INV} + P_{RES-INV}) \times \gamma_{INV}, \tag{5}$$

where P_{BA-INV} is the battery power injected to the inverter and also $P_{RES-INV}$ denotes renewable energy source power transmitted to the inverter.

3. Problem Formulation

This study uses the improved beluga whale optimization algorithm (IBWO) based on the inertia weight method to tackle the problem of operating 33- and real 59-bus distribution networks based on HMG scheduling and network reconfiguration while taking the self-healing improvement approach into consideration. The objective function of the issue and restrictions, the suggested method of optimization, and how it was used to resolve the issue are all provided in this part.

3.1. Objective Function

3.1.1. Power Losses. According to the current flowing through the network lines and accounting for their ohmic resistance and reactance, the network's total active power loss (P_L^T) is represented as follows [14, 16]:

$$P_L^T = \sum_{k=1}^{\varnothing} RES_k \times Cu_k^2, \qquad Cu_k = \frac{VOL_i - VOL_j}{RES_k + jREC_k}, \tag{6}$$

where RES_k and REC_k are the ohmic resistance and reactance of the line k, $\varnothing$ is the number of network lines, Cu_k is the current passing through the line k, and VOL_i and VOL_j are the voltage of buses i and j.

3.1.2. ENS. As a statement of the network subscribers' disrupted energy owing to the outage of the network lines, the reliability index in the form of energy not-supplied (ENS) can be described as follows [14, 16].

$$ENS_{NET}^{T} = \sum_{i=1}^{\varnothing} \sum_{j=1}^{NLL} RLO_i \times LL_i \times DLR_i \times \rho_i, \tag{7}$$

where ENS_{NET}^{T} is the total energy not-supplied of network subscribers, NLL is number of lost loads due to line outages or fault, RLO_i is the rate of line i outages, LL_i is the length of line i, DLR_i is the duration of line i repair, and ρ_i is the amount of lost load due to line i outages.

3.1.3. SAIDI. Another reliability index is the system average interruption duration index (SAIDI), which represents the average total duration of power outages per customer, which is computed as follows [14, 16]:

$$SAIFI = \frac{\sum(\lambda_i \times N_i)}{\sum N_i}, \tag{8}$$

where N_i represents the number of subscribers at load point i, λ_i represents the failure rate of load point i, and $U = \lambda \times r$, where r represents the outage time.

3.1.4. SAIFI. Another reliability index, the system average interruption frequency index (SAIFI) indicates the average number of power outages per customer, which is defined as follows [14, 16]:

$$SAIDI = \frac{\sum(U_i \times N_i)}{\sum N_i}. \tag{9}$$

3.1.5. HMG Cost. Minimizing the present value cost (NPC) of the HMG system, which includes investment costs (C_{INV}) and maintenance cost ($C_{OP\&M}$) over the system's useful life, is another goal. C_{INV} is the price of WTs, PVs, batteries, inverters, and $C_{OP\&M}$ related to WTs, PVs, and

batteries. The NPC is formulated as follows [30–32]:

$$\begin{aligned} \mathrm{NPC}_{\mathrm{HMG}} &= C_{\mathrm{INV}} + C_{\mathrm{OP\&M}}, \\ C_{\mathrm{INV}} &= (C_{\mathrm{PV}} \times n_{\mathrm{PV}}) + (C_{\mathrm{WT}} \times n_{\mathrm{WT}}) \\ &\quad + (C_{\mathrm{BA}} \times n_{\mathrm{BA}}) + (C_{\mathrm{INV}} \times n_{\mathrm{INV}}), \\ C_{\mathrm{OP\&M}} &= (C_{\mathrm{PV,OP\&M}} \times n_{\mathrm{PV}}) + (C_{\mathrm{WT,OP\&M}} \times n_{\mathrm{WT}}) \\ &\quad + (C_{\mathrm{BA,OP\&M}} \times n_{\mathrm{BA}}), \end{aligned} \tag{10}$$

where C_{PV}, C_{WT}, C_{BA}, and C_{INV} represent the purchase cost of each PV array, WT, battery, and inverter. n_{PV}, n_{WT}, n_{WT}, and n_{INV} indicate the number of PV arrays, WTs, batteries, and inverters. $C_{\mathrm{PV,OP\&M}}$, $C_{\mathrm{WT,OP\&M}}$, and $C_{\mathrm{BA,OP\&M}}$ also refer to the annual maintenance cost of PV arrays, WT, and batteries.

3.1.6. Multi-objective Optimization. The power loss minimization, enhancement of reliability indices, and reduction of HMG cost are all components of the problem's objective function. The weighting coefficient approach is formulated in this study to solve the total objective function with various dimensions as follows [33]:

$$\begin{aligned} F = \varphi_1 \times \left(\frac{P_L^T}{P_{L,\max}^T}\right) + \varphi_2 \times \left(\frac{\mathrm{ENS}_{\mathrm{NET}}^T}{\mathrm{ENS}_{\mathrm{NET,max}}^T}\right) + \varphi_3 \\ \times \left(\frac{\mathrm{SAIFI}}{\mathrm{SAIFI}_{\max}}\right) + \varphi_4 \times \left(\frac{\mathrm{SAIDI}}{\mathrm{SAIDI}_{\max}}\right) + \varphi_5 \\ \times \left(\frac{\mathrm{NPC}_{\mathrm{HMG}}}{\mathrm{NPC}_{\mathrm{HMG,max}}}\right), \end{aligned} \tag{11}$$

where φ_1, φ_2, φ_3, φ_4, and φ_5 are the weighting coefficients of losses, ENS, SAIFI, SAIDI, and HMG cost functions, respectively, such that the absolute value of their sum must be equal to 1. $P_{L,\max}^T$, $\mathrm{ENS}_{\mathrm{NET,max}}^T$, $\mathrm{SAIFI}_{\max}$, $\mathrm{SAIDI}_{\max}$, and $\mathrm{NPC}_{\mathrm{HMG,max}}$ refers to the maximum value of losses, ENS, SAIFI, SAIDI, and HMG cost.

3.2. Constraints. The prior subsection's objective function F should be optimized under the subsequent equality and inequality constraints [14, 16].

3.2.1. Power Balance.

$$P_{\mathrm{Post}} + \sum_{i=1}^{N_{\mathrm{HMG}}} P_{\mathrm{HMG}}(i) = \sum_{i=1}^{\varnothing} P_L(i) + \sum_{q=1}^{\vartheta} P_{\mathrm{Dmd}}(q), \tag{12}$$

$$Q_{\mathrm{Post}} + \sum_{i=1}^{N_{\mathrm{HMG}}} Q_{\mathrm{HMG}}(i) = \sum_{i=1}^{\varnothing} Q_L(i) + \sum_{q=1}^{\vartheta} Q_{\mathrm{Dmd}}(q), \tag{13}$$

where P_{Post} and Q_{Post} refer to the active and reactive power injected into the grid from the substation, P_{HMG} and Q_{HMG} refer to the active and reactive power transferred from the hybrid system into the grid, N_{HMG} indicates the number of hybrid systems (2 in this study), P_L and Q_L denote the active and reactive losses of the grid lines, and P_{Dmd} and Q_{Dmd} are the active and reactive load of the distribution network.

3.2.2. Bus Voltage. Bus i's voltage range must fall within the permitted range, which is as follows:

$$\mathrm{VOL}_{\min}^i \le \mathrm{VOL}^i \le \mathrm{VOL}_{\max}^i, \tag{14}$$

where $\mathrm{VOL}_{\min}^i$ and $\mathrm{VOL}_{\max}^i$ represent the lower and upper network bus voltages.

3.2.3. Maximum Allowable Currents. Line i's current must be below its limit to cross through:

$$\mathrm{Cu}^i \le \mathrm{Cu}_{\max}^i, \tag{15}$$

where $S_i^{\max}$ is the upper current passing through the lines.

3.2.4. HMG Components. Equipment for HMG systems must have the following maximum and minimum ranges [30–32]:

$$n_{\mathrm{PV}}^{\min} \le n_{\mathrm{PV}} \le n_{\mathrm{PV}}^{\max}, \tag{16}$$

$$n_{\mathrm{WT}}^{\min} \le n_{\mathrm{WT}} \le n_{\mathrm{WT}}^{\max}, \tag{17}$$

$$n_{\mathrm{BA}}^{\min} \le n_{\mathrm{BA}} \le n_{\mathrm{BA}}^{\max}, \tag{18}$$

$$E_{\mathrm{BA}}^{\min} \le E_{\mathrm{BA}} \le E_{\mathrm{BA}}^{\max}, \tag{19}$$

where $n_{\mathrm{PV}}^{\min}$ and $n_{\mathrm{PV}}^{\max}$ are the lower and upper numbers of PV panels, $n_{\mathrm{WT}}^{\min}$ and $n_{\mathrm{WT}}^{\max}$ refer to the minimum and upper numbers of WTs, $n_{\mathrm{BA}}^{\min}$ and $n_{\mathrm{BA}}^{\max}$ represent the lower and upper numbers of batteries, $E_{\mathrm{BA}}^{\min}$ and $E_{\mathrm{BA}}^{\max}$ indicate the lower and upper energies of the battery as $E_{\mathrm{BA}}^{\min} = (1 - \mathrm{DOD}) \times E_{\mathrm{BA}}^{\max}$, and DOD indicates the depth of battery discharge.

3.2.5. Network Radiality. The distribution network's radial state should be preserved as follows during network reconfiguration. In order to verify the network's radiality, an incidence matrix is first defined. There are m network lines and n network buses in this matrix, which is a m by n matrix. If the determinant of this matrix decreases to zero after it is formed, the network is not a radial network; if it means $\det(A) = 1$ or -1, the network is a radial network [34].

4. Optimization Method and Implementation

The operation of a 33- and 59-bus distribution networks based on multi-HMG scheduling and network reconfiguration taking self-healing into account is discussed in this part. It is solved using the enhanced beluga whale optimization (BWO) algorithm based on the inertia weight method (IBWO) [28]. Beluga whale actions like swimming, hunting, and falling are the inspiration for the BWO.

4.1. Inspiration. The beluga whale, a marine mammal, is identified based on its white pigmentation and diversified utterances. Several belugas are maintained in aquariums in which they exhibit an energetic look and smooth motion.

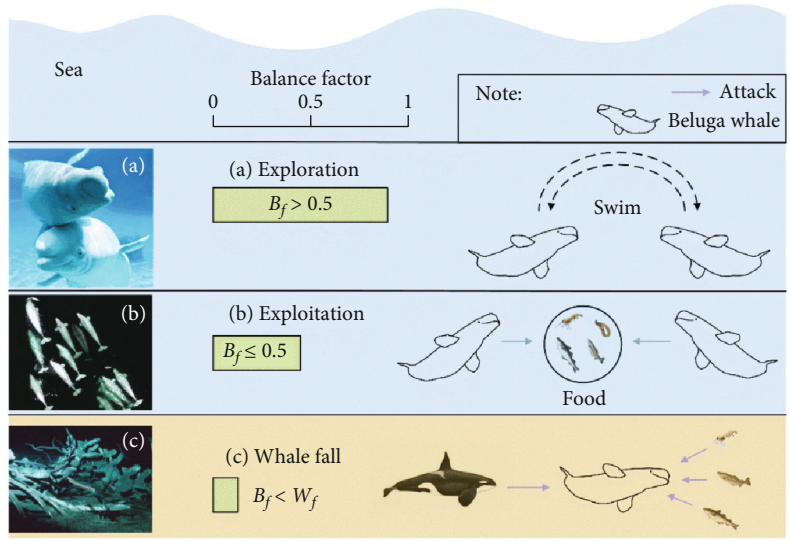

FIGURE 2: Beluga whale behaviors: (a)—swimming, corresponding to the exploration phase; (b)—feeding, responding to the exploitation phase; (c)—whale fall, corresponding to the whale fall phase [28].

Some belugas are maintained in aquariums, as depicted in Figure 2(a), and they have a cheerful appearance and graceful movement. The social-sexual behaviors of beluga whales under human care include lateral and vertical swimming, synchronized submersion, and synchronized milling. Moreover, they may explode bubbles, open their mouths to eat, and swim rapidly towards or away from other creatures. Beluga whales are interested in humans and demonstrate activities such as frolicking, swimming, and vocalization. Beluga whales are social animals that can congregate in groups of two to twenty-five individuals, on average ten individuals. They consume a variety of prey, such as crustaceans, nematodes, codfish, trout, and salmon (Figure 2(b)). Due to the dense population density in estuaries, killer whales, polar bears, and humans pose a threat to these animals. Over immigration, whales perish and sink to the ocean floor, providing sustenance for many different things (Figure 2(c)) [28].

The beluga whale optimization (BWO) is affected by beluga whales' swimming, foraging, and falling actions. This is how the BWO mathematical model is created.

4.2. Mathematical Model. The BWO mimics the swimming and other actions of beluga whales and foraging. Similar to other metaheuristics, BWO is comprised of the exploration and exploitation phases. Through the arbitrary choice of beluga whales, the discovery phase enables global looking in the layout space, whereas the exploitation phase governs local searching. For modeling the actions of beluga whales, it is assumed that they are search agents that can move in search space by modifying their position vectors. Moreover, BWO incorporates the chance of whale collapse, which adjusts the corresponding positions of beluga whales [28].

Because of BWO's population-centered methodology, beluga whales are seen as searching agents, and each one represents a potential solution that has undergone overoptimization. The following is the layout of the agent location discovery matrix [28]:

$$X = \begin{bmatrix} x_{1,1} & x_{1,2} & \cdots & x_{1,d} \\ x_{2,1} & x_{2,2} & \cdots & x_{2,d} \\ \vdots & \vdots & & \vdots \\ x_{n,1} & x_{n,2} & \cdots & x_{n,d} \end{bmatrix}, \tag{20}$$

where d is the dimension of design variables and n is the beluga whale population size. Several physiological parameters have been collected for every living beluga whale [28]:

$$F_X = \begin{bmatrix} f(x_{1,1}, x_{1,2}, \cdots, x_{1,d}) \\ f(x_{2,1}, x_{2,2}, \cdots, x_{2,d}) \\ \vdots \quad \vdots \quad \vdots \\ f(x_{n,1}, x_{n,2}, \cdots, x_{n,d}) \end{bmatrix}. \tag{21}$$

Based on the equilibrium factor B_f, the BWO algorithm is capable of switching within both discovery and extraction by [28]

$$B_f = B_0 \times \left(\frac{1 - T}{(2 \times T_{\max})} \right). \tag{22}$$

At each iteration, where T denotes the present iteration and $T_{\max}$ refers to the maximum number of iterations, B_0 varies arbitrarily between 0 and 1. Discovery happens when B_f is greater than 0.5, whereas exploitation happens when B_f is less than 0.5. Rising iteration T decreases the fluctuation range of B_f from (0, 1) to (0, 0.5), indicating an important change in likelihood for both the exploration and the exploitation phases, whereas growing iteration T raises the probability of the discovery phase.

4.2.1. Exploration Phase. The BWO exploration phase is determined by analyzing beluga whales' swimming activity. According to documented habits of beluga whales in human care, beluga whales may participate in social-sexual behaviors from a variety of positions, such as the coordinated or reversed pair swim portrayed in Figure 1. Thus, the precise positions of investigators are established by the tandem swim of beluga whales, and the geographic coordinates of beluga whales are altered to reflect this [28]:

$$\begin{cases} X_{i,j}^{T+1} = X_{i,j}^{T} + \left(X_{r,p_1}^{T+1} - X_{i,p_j}^{T}\right)(1 + r_1)\sin(2\pi r_2), & j = \text{even}, \\ X_{i,j}^{T+1} = X_{i,j}^{T} + \left(X_{r,p_1}^{T+1} - X_{i,p_j}^{T}\right)(1 + r_1)\sin(2\pi r_2), & j = \text{even}, \end{cases} \tag{23}$$

where T represents the iteration quantity, $X_{i,j}^{T+1}$ indicates the new positioning of the ith beluga whale in the jth dimension, p_j $(j = 1, 2, \cdots, d)$ is a number chosen at random representing the d-dimension, and $X_{i,pj}^{T}$ is the new positioning of the ith beluga whale in the p_j dimension. T is the position of the ith beluga whale on the p_j dimension, $X_{i,pj}^{T}$ and $X_{r,p1}^{T}$ refer to the current coordinates of the ith and rth beluga whales (r is a beluga whale selected at random), and T is the place of the ith beluga whale on the p_j dimension. r_1 and r_2 are arbitrary integers between 0 and 1, and the functions $\sin(2\pi r_2)$ and $\cos(2\pi r_2)$ show that the beluga whales' flippers are facing upwards. The revised positioning reflects the coordinated or mirror-like swimming and diving behaviors of beluga whales depending on the dimension chosen via an odd and even quantity. Two random integers, r_1 and r_2, are used to enhance randomized operators during the exploratory stage.

4.2.2. Exploitation Phase. The BWO exploiting phase is affected via beluga whales' predatory tendencies. Beluga whales have the capability of coordinated eating and locomotion when other beluga whales are nearby. Therefore, beluga whales prey by exchanging information about positions that are open, while taking into consideration the best competitor and others as well. During the predatory period of BWO, the Levy flight [28] method is applied in order to increase convergence. We postulated that such creatures could secure their prey by employing the Levy flying tactics, and the associated framework is presented as follows [28]:

$$X_{i,j}^{T+1} = r_3 X_{\text{best}}^{T} - r_4 X_i^{T} + C_1 . L_F . \left(X_r^{T} - X_i^{T}\right), \tag{24}$$

where T is the present iteration, X_i^T is the present location of the ith beluga whale, X_r^T is the current situation of an arbitrary beluga whale, X_i^{T+1} is the most recent position of the ith beluga whale, and X_{best}^{T} is the present location of the best beluga whale. r_3 and r_4 are indeterminate values between (0 and 1), and $C_1 = 2r_4(1 - T/T_{\max})$ is the randomized jump power that determines the Levy flight power.

The Levy flight formula is calculated in the following way [28]:

$$L_F = 0.05 \times \frac{u \times \sigma}{|v|^{1/\beta}}, \qquad \sigma = \left(\frac{\Gamma(1+\beta) \times \sin(\pi\beta/2)}{\Gamma((1+\beta)/2) \times \beta \times 2^{(\beta-1)/2}}\right)^{1/\beta}, \tag{25}$$

where u and v are random quantities with a normal distribution and β equates to the fixed 1.5.

4.2.3. Whale Fall. Beluga whales are threatened by predators such as killer whales, polar bears, and humans throughout passage and feeding. The majority of beluga whales are clever and are able to prevent peril by sharing information. Nonetheless, a few beluga whales passed away and fell into the ocean abyss. The phenomenon is referred to as "whale fall," and it provides sustenance for an extensive variety of animals. Countless predators and invertebrates converge on whale corpses in search of sustenance, and the fractured skulls and corpses of dead whales drew an extensive amount of hairy crabs. The skeleton is gradually destroyed or inhabited for many years by microorganisms and algae [28].

To simulate the actions of whales falling during every iteration, we arbitrarily select the likelihood of whale decline from the individuals in the population to simulate minor differences in the sets. We believe that these beluga whales either moved to another spot or received shots and plunged into the depths of the sea after being wounded. In order to keep the identical amount of population, the current positions of beluga whales and the whale fatality step size are employed to figure out the revised position. This is how the model is presented as follows [28]:

$$X_i^{T+1} = r_5 X_i^{T} - r_6 X_i^{T} + r_7 X_{\text{step}}, \tag{26}$$

where r_5, r_6, and r_7 are random integers ranging from 0 to 1 and X_{step} is the step dimension of whale descent determined by [28].

$$X_{\text{step}} = (u_b - l_b)\exp\left(\frac{-C_2 T}{T_{\max}}\right), \tag{27}$$

where C_2 is the step element related to whale fatality and the size of the population ($C_2 = 2\,W_f \times n$) and u_b and l_b are the upper and lower variable bounds, respectively. The amount of steps is determined by the maximum number of scheduling variables and iterations.

This model estimates the likelihood of whale stranding (W_f) as a function that is linear [28].

$$W_f = 0.1 - \frac{0.05T}{T_{\max}} \tag{28}$$

The reality that the possibility of whale plummet dropped from 0.1 in the first iteration to 0.05 in the final iteration indicates that, as beluga whales become closer to

sources of protein over the optimization process, their vulnerability reduces.

4.3. The BWO Procedure. Depending on the previous principle, BWO consists of three phases: the exploration phase, which simulates floating behavior; the predatory phase, which simulates killing behavior; and the whale collapse phase, which is modified by the beluga whale's decline. Every time the optimization procedure is repeated, when the stages of exploration and extraction draw the conclusion, the whale decline phase begins to occur. The final section describes the principal BWO method.

Step 1 (initialization). Establish the BWO specifications, including the population amount n and the maximum number of iterations $T_{\max}$. The primary locations of every beluga whale within the search space were chosen at random, and values for fitness can be calculated using the fitness.

Step 2 (update the exploration and discovery procedure). The equilibrium factor B_f decides how much a beluga whale will go through the stage of exploration or utilization phase. If B_f for a beluga whale is greater than 0.5, the revision method enters the searching phase, and the beluga whale's position is updated. If B_f is less than 0.5, the stage of exploitation governs the revisions, and the exact position of a beluga whale is updated. Taking this, the fitness ratings of the newly created positions are obtained and ordered to find the best one for the present iteration.

Step 3 (updates on the phase of whale lactation). Each iteration estimates the whale descent possibility W_f. Multiple beluga whales may perish and sink to the ocean floor, and the whale descent probability W_f is computed with each iteration. Consequently, update the location of a beluga whale.

Step 4 (verification of conditioned ending). The BWO ends if a specific iteration surpasses the maximum number of iterations. Optionally, repeat Step 2.

4.4. Overview of the Improved BWO (IBWO). A nonlinearly diminishing inertia weight approach [29] is used to improve both the local and global exploratory results for conventional BWO. Variations in IW value impact the capability to search. From $\mathrm{IW}_{\max}$ to $\mathrm{IW}_{\min}$, the IW declined in a nonlinear manner. Large IW values have been advantageous for locating global advances, whereas small IW values are suitable for locating regional breakthroughs. This approach is outlined by [29]

$$\mathrm{IW} = \mathrm{IW}_{\min} + \left(\frac{1+\cos\left(\pi t/T\right)}{2}\right)^{\mathrm{pc}} \left(\mathrm{IW}_{\max} - \mathrm{IW}_{\min}\right), \quad (29)$$

where $\mathrm{IW}_{\max}$ and $\mathrm{IW}_{\min}$ are the utmost and smallest IW amounts, respectively. T is the maximum number of iterations, and pc is a positive number (pc = 10 [29]).

The info that follows has been modified:

$$\begin{cases} X_{i,j}^{T+1} = \left(\mathrm{IW}_{\min} + \left(\dfrac{1+\cos\left(\pi t/T\right)}{2}\right)^{\mathrm{pc}} \left(\mathrm{IW}_{\max} - \mathrm{IW}_{\min}\right)\right) \times X_{i,j}^{T} + \left(X_{r,p_1}^{T+1} - X_{i,p_j}^{T}\right)(1+r_1)\sin\left(2\pi r_2\right), & j = \text{even}, \\ X_{i,j}^{T+1} = \left(\mathrm{IW}_{\min} + \left(\dfrac{1+\cos\left(\pi t/T\right)}{2}\right)^{\mathrm{pc}} \left(\mathrm{IW}_{\max} - \mathrm{IW}_{\min}\right)\right) \times X_{i,j}^{T} + \left(X_{r,p_1}^{T+1} - X_{i,p_j}^{T}\right)(1+r_1)\sin\left(2\pi r_2\right), & j = \text{even}. \end{cases} \quad (30)$$

4.5. The IBWO Implementation. Flowchart of the IBWO implementation to solve the problem is depicted in Figure 3. The steps of the problem implementation using the IBWO are as follows:

Step 1. The program provides details regarding the 33-bus distribution network, such as ohmic resistance and reactance values for network, active, and reactive demand; the lowest and highest ratings for PVs, WTs, and batteries; and the network's tie-line quantity.

Step 2. Establishing the algorithm's parameters, such as the size of population and maximal iteration of the IBWO, as well as the total amount of beluga whales.

Step 3. For the starting point of the algorithm, the variables consist of the location and size of the HMG system devices (the installation location of buses 2 to 33 and the maximum capacity of the number of PVs, WTs, and batteries 500, 500, and 3000, respectively) in addition to the network open switches (the number of 5 switches to be a variable among 37 network lines (plus tie-lines) chosen at random corresponding to the range of v).

Step 4. The decision variable sets for the algorithm population are found, randomly.

Step 5. The backward-forward power flow is done, and the value of the objective function (Eq. (11)) is computed for the variable set, taking into consideration the operational and HMG constraints (Eqs. (12)–(19)) along with the network radial status. This phase identifies the optimum variable set considering the objective function (Eq. (11)) value.

Step 6. Update the BWO population.

Step 7. The computation of the value of the objective function (Eq. (11)) per revised population in step by step 6, witnessing operation limitations the size of resources and batteries, and the condition to preserve the radial state of the network, and changing it with the previous set (step 5) if the new variables have better outcomes (better value be subject to the objective).

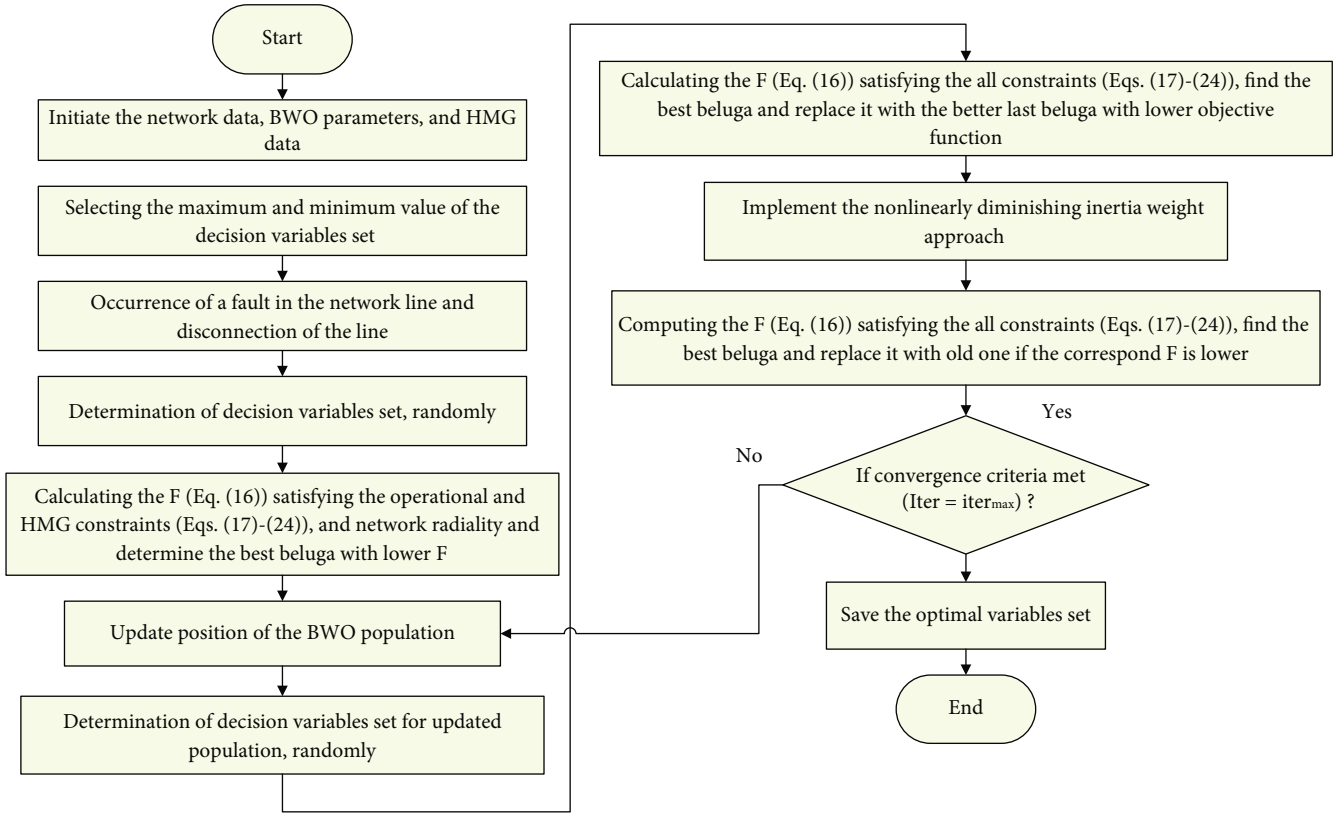

Figure 3: Flowchart of the IBWO implementation to solve the problem.

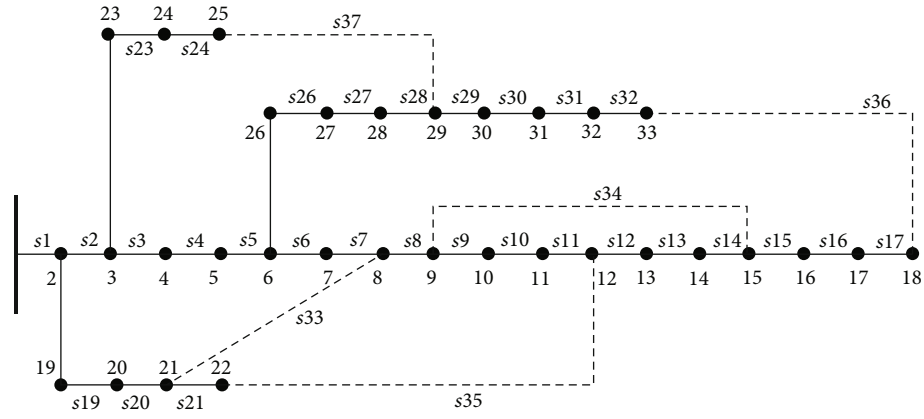

Figure 4: The 33-bus distribution network.

Step 8. In this stage, the traditional BWO population is updated based on the inertia weight method (IBWO).

Step 9. The objective function (Eq. (11)) value for each updated set is computed in step 8, and the value of the superior answer is substituted with the best variable value set from step 7.

Step 10. Evaluation of convergence requirements (under the condition of obtaining the best objective function (Eq. (11)) and performing the greatest number of algorithm iterations). If yes, proceed to step 11; if not, proceed to step 6.

Step 11. Terminate the procedure and print the optimal variable set, which includes the place of installation and size of the HMGs' component as well as open network switches.

5. Simulation Results and Discussion

In this section, the results of the operation and reconfiguration of a 33- and 59-bus distribution networks with HMG multi-HMG operation and self-healing enhancement via the improved beluga whale optimization (BWO) algorithm based on the inertia weight method (IBWO) are presented. Figure 4 displays the network schematic for the 33-bus network. This network has 37 branches and 5 tie-lines, identified as lines 33, 34, 35, 36, and 37, with a total active demand of 3,720 kW and a reactive demand of 2,300 kVAr. Also, a real 59-bus distribution network is considered to implement the proposed methodology and is depicted in

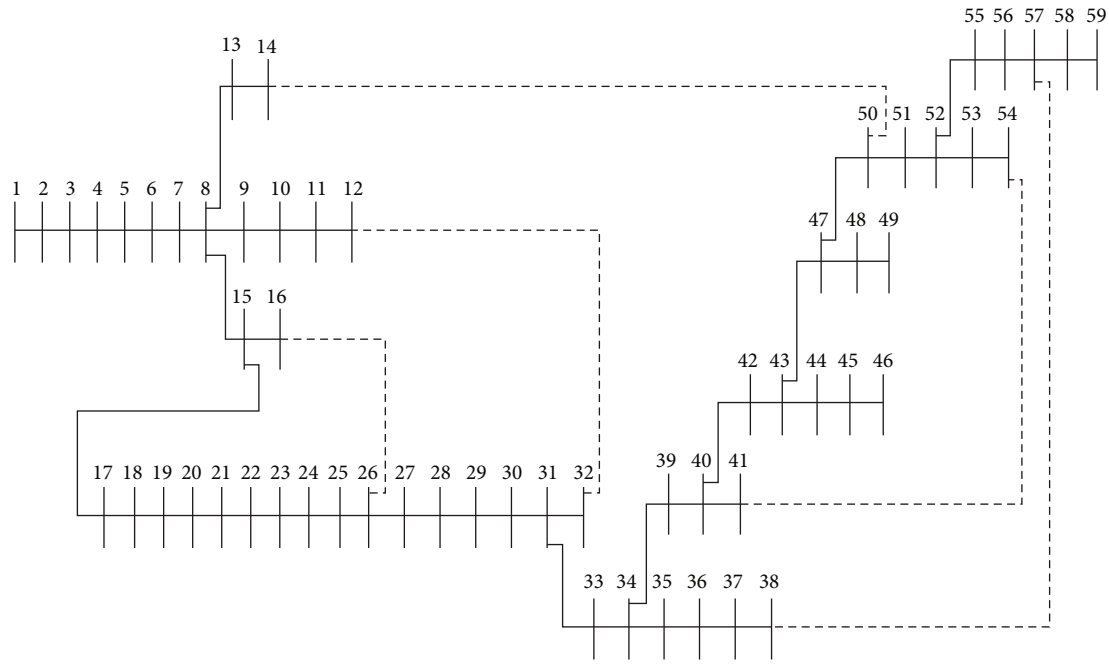

Figure 5: The real 59-bus distribution network.

Figure 5. This network is a section of the southern Iranian city of Ahvaz's distribution network. There are 63 branches, 5 tie-lines identified as lines 59, 60, 61, 62, and 63, and 58 sectionalizing switches in the 59-bus distribution network with 9,690 kW and 7,318.2 kVAr, respectively, represent the total active and reactive demands. The bus and line data of the real 59-bus network is presented in Table 2. The network loading data from Ref. [35] is displayed in Figure 6. In addition, meteorological data, such as solar radiation data, ambient temperature data, and wind speed data, were extracted based on Ref. [31] and presented in Figures 7–9. In addition, Table 3 provides data on numerous HMG equipment. To validate the IBWO solver, its efficacy in solving the operation problem was compared to that of the traditional BWO method particle swarm optimization (PSO) and ant lion optimizer (ALO). In all simulations, the size of population, maximum iteration number, and number of autonomous executions of each method are tuned to 50, 200, and 25, correspondingly. Moreover, the general and regulatory parameters of BWO, PSO, and ALO have been chosen as per each algorithm's respective reference paper. The simulation of the recommended approach was performed in the MATLAB software using a desktop system with an Intel Core i7, 8 GB of memory, and a 1 TB hard disk drive.

For the purpose of assessing the efficacy of the proposed methodology, the following scenarios have been executed:

Scenario #1. Network operation based on scheduling of a HMG without SH.

Scenario #2. Network operation based on scheduling of two HMGs without SH.

Scenario #3. Network operation based on reconfiguration without SH.

Scenario #4. Network operation based on the scheduling of a HMG and reconfiguration without SH.

Scenario #5. Network operation based on scheduling of two HMGs and reconfiguration without SH.

Scenario #6. Network operation based on scheduling of two HMGs and reconfiguration with SH.

5.1. The Simulation Results without SH, 33-Bus Network

5.1.1. The Results of Scenario #1. The results of a 33-bus distribution network with the HMG scheduling without SH consideration using the IBWO algorithm are given. The efficacy of IBWO to solve the problem is compared to that of BWO, PSO, and ALO. Evidently, the IBWO procedure has attained the optimal solution with a faster convergence rate (Figure 10). On the other hand, it can be seen that enhancing the capability of the traditional BWO algorithm based on the inertial weight method improves its discovery achievement and prevents premature convergence to the extent that the enhanced version has achieved convergence in fewer convergence iterations than its traditional counterpart.

Table 4 displays the numerical outcomes of the operation of a 33-bus distribution network based on the scheduling of an HMG without consideration of SH via the IBWO. Based on backward-forward load flow, the ENS, SAIFI, and SAIDI values for the base network are obtained 1824.79 kWh, 53.93 MWh, 4.10, and 48.65, respectively. The IBWO has attained a lower objective function value (better performance) than the BWO, PSO, and ALO techniques. The IBWO method installed 2 PVs, 252 WTs, and 17 batteries in bus 33, as shown in Table 4. The energy losses, ENS, SAIFI, SAIDI, and HMG costs are 1275.12 kWh, 44.77 MWh, 2.06, 32.36, and 65,576.17

Table 2: The load and line data of real 59-bus distribution network.

Line	Sending bus	Ending bus	R (ohm)	X (ohm)	P (kW)	Q (kVAr)
1	1	2	0.081	0.061	72	54
2	2	3	0.135	0.101	51	38.25
3	3	4	0.027	0.020	50	37.50
4	4	5	0.027	0.020	50	37.50
5	5	6	0.027	0.020	85	63.75
6	6	7	0.027	0.020	108	81
7	7	8	0.540	0.405	0	0
8	8	9	0.540	0.405	80	60
9	9	10	0.270	0.203	320	240
10	10	11	0.540	0.405	288	216
11	11	12	0.540	0.405	125	93.75
12	8	13	0.027	0.020	108	81
13	13	14	0.027	0.020	200	150
14	8	15	0.027	0.020	0	0
15	15	16	0.027	0.020	95	71.25
16	15	17	0.027	0.020	200	150
17	17	18	0.027	0.020	225	168.75
18	18	19	0.027	0.020	100	75
19	19	20	0.027	0.020	231	173.25
20	20	21	0.027	0.020	410	307.50
21	21	22	0.027	0.203	450	337.50
22	22	23	0.027	0.020	230	172.50
23	23	24	0.027	0.020	262	196.50
24	24	25	0.027	0.020	250	187.50
25	25	26	0.027	0.203	400	310.43
26	26	27	0.027	0.020	203	152.25
27	27	28	0.027	0.020	200	150
28	28	29	0.027	0.020	320	240
29	29	30	0.027	0.020	200	150
30	30	31	0.027	0.020	260	199.50
31	31	32	0.027	0.020	240	186.26
32	31	33	0.135	0.101	150	112.50
33	33	34	0.027	0.020	0	0
34	34	35	0.054	0.041	158	118.50
35	35	36	0.027	0.020	40	30
36	36	37	0.027	0.020	190	142.50
37	37	38	0.027	0.020	87	65.25
38	34	39	0.027	0.020	450	337.50
39	39	40	0.027	0.020	0	0
40	40	41	0.054	0.041	420	315
41	40	42	0.054	0.041	100	75
42	42	43	0.027	0.020	0	0
43	43	44	0.027	0.020	199	149.25
44	44	45	0.027	0.020	80	60
45	45	46	0.027	0.020	420	315
46	43	47	0.027	0.203	0	0
47	47	48	0.027	0.020	141	105.75
48	48	49	0.027	0.203	165	123.75
49	47	50	0.027	0.020	0	0
50	50	51	0.027	0.020	300	225
51	51	52	0.027	0.020	0	0
52	52	53	0.027	0.020	100	80.23
53	53	54	0.081	0.061	178	133.50
54	52	55	0.54	0.405	0	0
55	55	56	0.135	0.101	235	176.25
56	56	57	0.054	0.041	154	123.55
57	57	58	0.027	0.020	0	0
58	55	59	0.054	0.041	310	248.71
59	16	26	0.50	0.50	—	—
60	14	50	0.50	0.50	—	—
61	12	32	0.50	0.50	—	—
62	38	57	0.50	0.50	—	—
63	41	54	0.50	0.50	—	—

dollars, respectively. By obtaining lower values of energy losses, ENS, SAIFI, and SAIDI, the IBWO method has a better performance in network operation according to the scheduling of an HMG, as a consequence of reducing the energy of network subscribers, as determined by a comparison of the results of various methods. As a result of the HMG system's regularly scheduled energy injection, the network's dependability has been enhanced.

5.1.2. The Results of Scenario #2. The results of a 33-bus network with the scheduling of two HMGs without considering SH using the IBWO algorithm are given. The capability of the IBWO method to solve the problem is compared with the traditional algorithms of BWO, PSO, and ALO. As can be seen in Figure 11, the IBWO method has achieved the optimal solution with a higher convergence speed. On the other hand, it is clear that improving the performance of the traditional BWO algorithm based on the inertial weight method strengthens its discovery performance and prevents premature convergence in such a way that the improved version has achieved convergence in fewer repetitions of convergence compared to its traditional version.

The numerical results of the operation of a 33-bus distribution network based on the scheduling of two HMGs without considering SH using the IBWO are presented in Table 5. As can be seen, the IBWO method has achieved a lower objective function value compared to the BWO, PSO, and ALO methods. According to Table 5, the IBWO method installed one HMG with 1 PV, 180 WTs, and 75 batteries in bus 33 and another HMG in bus 15 with 284 PVs, 395 WTs, and 570 batteries. With the optimal scheduling of two HMGs, the amount of energy loss, ENS, SAIFI, SAIDI, and HMG cost is 963.06 kWh, 27.58 MWh, 2.75, 37.84, and \$155,445.61, respectively. The comparison of the results of different methods showed that the IBWO method by achieving lower values of energy losses, ENS, SAIFI, and SAIDI has a better performance in network

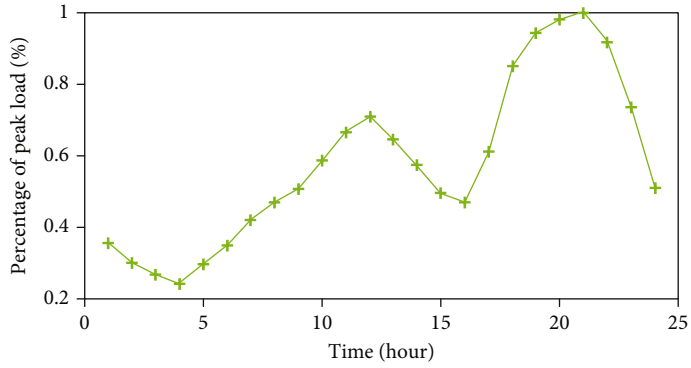

Figure 6: Network loading during a day.

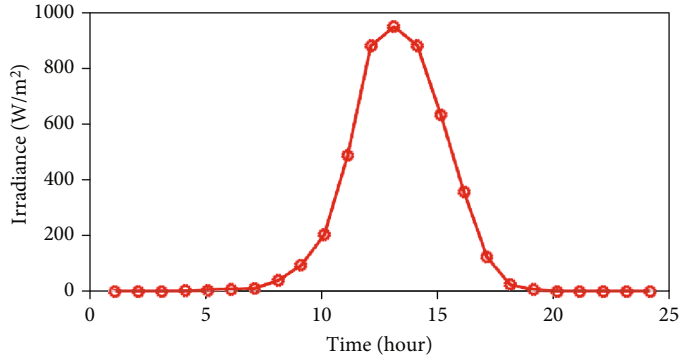

Figure 7: Irradiance profile during a day.

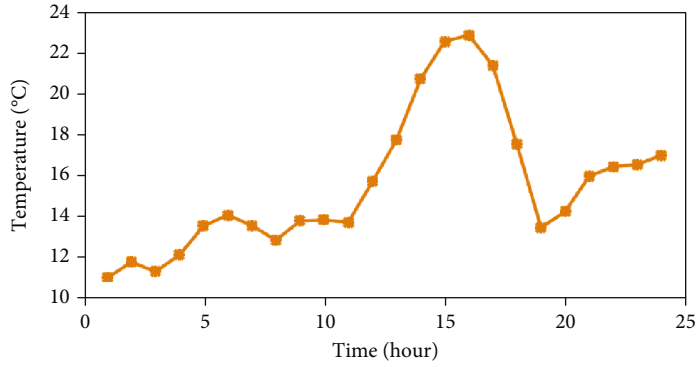

Figure 8: Temperature profile during a day.

operation based on the scheduling of two HMGs, as it is caused by reducing the energy of network subscribers. In the planned energy injection of the microgrid system, it has also improved the reliability level of the network.

5.1.3. The Results of Scenario #3. In this section, the IBWO algorithm-based operation results of a 33-bus distribution network based on reconfiguration are presented without considering SH. The efficacy of IBWO in solving the problem was compared to that of BWO, PSO, and ALO. All optimization techniques have converged on the optimal value according to Figure 12. The IBWO method, on the other hand, has obtained the optimum solution with the more convergence rate and faster convergence iteration than other methods.

In addition, Table 6 presents the numerical results of the operation of the 33-bus network based on reconfiguration without consideration of SH using various algorithms. As can be seen, the energy losses, ENS, and SAIFI values for each method are 1283.77 kWh, 43.84 MWh, 3.38, and 42.89, respectively. In the reconfiguration problem, the IBWO method has obtained the configuration of the network optimally, by opening switches 7, 10, 14, 28, and 32.

5.1.4. The Results of Scenario #4. Using the IBWO, the outcomes of operating a 33-bus network according to the

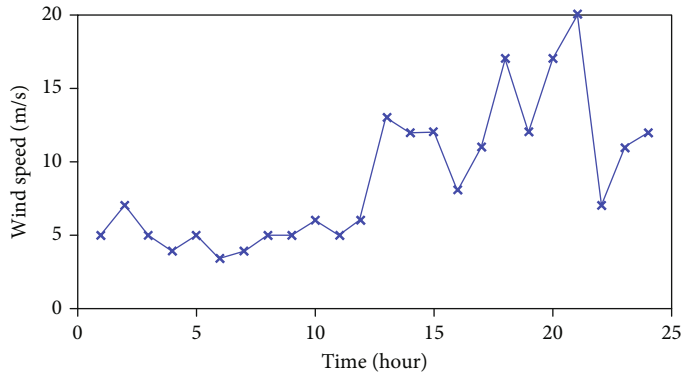

Figure 9: Wind speed profile during a day.

Table 3: The hybrid HMG system component data [31, 36].

Device	Item	Value
PV array	Rated power	1 kW
	Ref. irradiance	1000 W/m^2
	Ref. temperature	25$^{\circ c}$
WT	Nominal power	1 kW
	Cut-in wind speed	3 m/s
	Cut-out wind speed	9 m/s
	Rated wind speed	20 m/s
Battery	Maximum size	1 kWh
	Minimum size	0.2 kWh
	Charge efficiency	90%
	Discharge efficiency	90%
	DOD	0.8
Inverter	Efficiency	95%

scheduling of an HMG and network reconfiguration without taking into account SH are presented in this section. The efficacy of IBWO to solve the problem is contrasted to that of BWO, PSO, and ALO. Evidently, the IBWO procedure has attained the optimal solution with a faster convergence rate (Figure 13). On the other hand, it can be noticed that enhancing the traditional BWO performance relying on the inertial weight approach improves its discovery profitability and hinders premature convergence, such that the improved version reached convergence in fewer convergence iterations than the conventional version.

Table 7 gives the numerical outcomes of the operation of a 33-bus distribution network determined by the scheduling of an HMG with network reconfiguration and disregarding SH with the IBWO. The IBWO identifies the optimum configuration by opening switches 7, 10, 14, 16, and 28 and taking into account the place of installation of the HMG in bus 17 so that the number of PVs, WTs, and batteries is correspondingly 12, 156, and 80. Energy losses, ENS, SAIFI, SAIDI, and HMG expenses are 1150.46 kWh, 37.94 MWh, 2.07, 32.42, and 42,019.63 dollars, respectively, based on the IBWO method's determination of the decision variables. The results gathered by various methods indicate that each method succeeded in creating an optimal network configuration that is distinct from the others and has also provided the implementation location and various capacities of the HMG. As with previous comparisons, the results demonstrate the superior performance of the IBWO method in achieving multiple objectives, such as decreasing energy losses and increasing reliability metrics.

Figure 14 depicts the variations in the generated power of PVs and WTs, in addition to the planned power injection by HMG into the 33-bus network. The HMG, which depends on the management of battery storage charge and discharge, proved enabled to inject continuous and predetermined power into the distribution network. The battery storage system stores extra power to satisfy the load's requirements and releases the stored reserve energy in moments of power deficit from renewable resources in order to reliably supply the demand.

Figures 15 and 16 depict the variations in network power loss and ENS before and after HMG scheduling and network reconfiguration over the course of 24 hours. As demonstrated in scenario 4, network power losses, particularly peak load, have dropped based on the planned injection of HMG power, network reconfiguration, and load flow path modifications, from 1824.79 kWh to 1150.46 kWh in the base network. Also, in Figure 16, the customer energy not-supplied is decreased during all hours, which is a result of battery storage power management in the HMG system. As a result, the network's reliability has increased, and the value of ENS has decreased from 53.93 MWh to 37.9 MWh.

Figure 17 depicts the voltage profile curve of the 33-bus network before and after scheduling an HMG and network reconfiguration. It is evident that after resolving the scheduling problem, the network voltage deviations decreased, resulting in an enhanced profile of voltages.

5.1.5. The Results of Scenario #5. The outcomes of the network operation based on the scheduling of two HMGs and network reconfiguration are given without considering SH using the IBWO algorithm. The IBWO performance is compared with BWO, PSO, and ALO. In Figure 18, it is clear in this scenario that the IBWO has reached the convergence and optimal solution sooner than other methods and has achieved the lower objective function value.

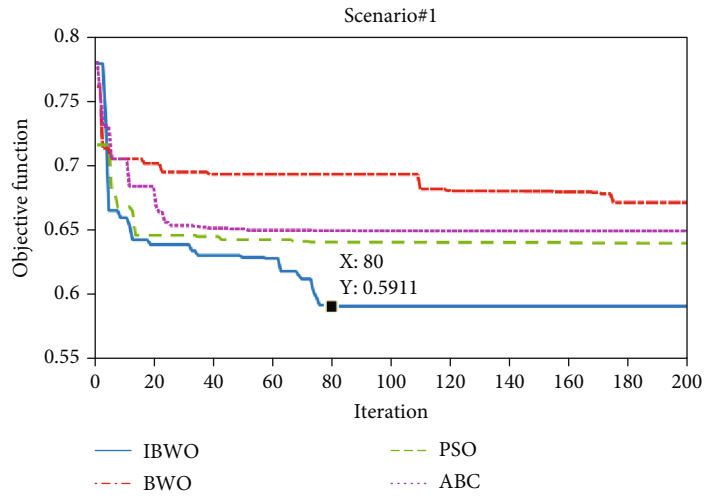

Figure 10: Convergence process of different methods for scenario 1.

Table 4: Numerical results of scenario 1 (one HMG) using different optimization methods.

	Base net	IBWO	BWO	PSO	ALO
HS location (bus)	—	Bus 33	@ 13	@ 16	Bus 13
PV size (kW)	—	2	0	0	25
WT size (kW)	—	252	190	164	171
Battery size (kWh)	—	17	100	646	86
Power losses (kW)	1824.79	1275.12	1608.63	1480.04	1531.79
ENS (MWh/yr)	53.93	44.77	46.182	46.537	46.963
SAIFI (failure/customer/yr)	4.10	2.06	2.50	2.39	3.31
SAIDI (hour/customer/yr)	48.65	32.36	35.84	35.01	42.32
HMG cost ($)	—	65,576.17	51,390.12	44,328.11	44363.39
OF	—	0.5910	0.6493	0.6399	0.6714

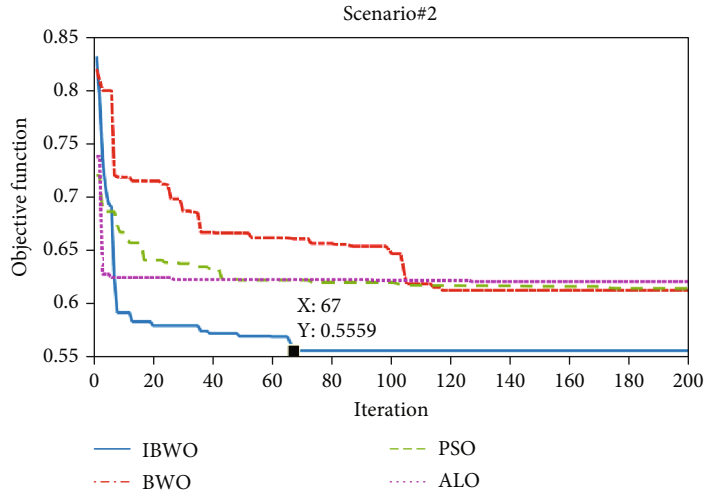

Figure 11: Convergence process of different methods for scenario 2.

The scheduling results of two HMGs and network reconfiguration are presented without considering SH using the IBWO algorithm in Table 8. The IBWO method determines the best network configuration by opening switches 7, 10, 14, 16, and 28 and determines the site of the first HMG in bus 33 such that the number of PVs, WTs, and batteries is 14, 174, and 22, respectively, and the location. The installation of the second HMG is determined in bus 17, as the PV,

Table 5: Numerical results of scenario 2 (two HMGs) using different optimization methods.

	Base net	IBWO	BWO	PSO	ALO
HS_1 location (bus)	—	Bus 33	Bus 11	@ 27	Bus 16
PV_1 size (kW)	—	1	46	144	1
WT_1 size (kW)	—	180	251	295	163
$Battery_1$ size (kWh)	—	75	23	834	10
HS_2 location (bus)	—	Bus 15	Bus 28	@ 16	Bus 2
PV_2 size (kW)	—	284	494	54	74
WT_2 size (kW)	—	394	497	342	3
$Battery_2$ size (kWh)	—	570	1121	2160	105
Power losses (kW)	1824.79	963.06	808.81	919.57	1640.09
ENS (MWh/yr)	53.93	27.58	30.666	28.156	46.752
SAIFI (failure/customer/yr)	4.10	2.75	3.11	3.15	2.41
SAIDI (hour/customer/yr)	48.65	37.84	40.72	41.05	35.13
HMG cost ($)	—	155,445.61	203,196.82	172,812.74	43160.00
OF	—	0.5559	0.6122	0.6140	0.6204

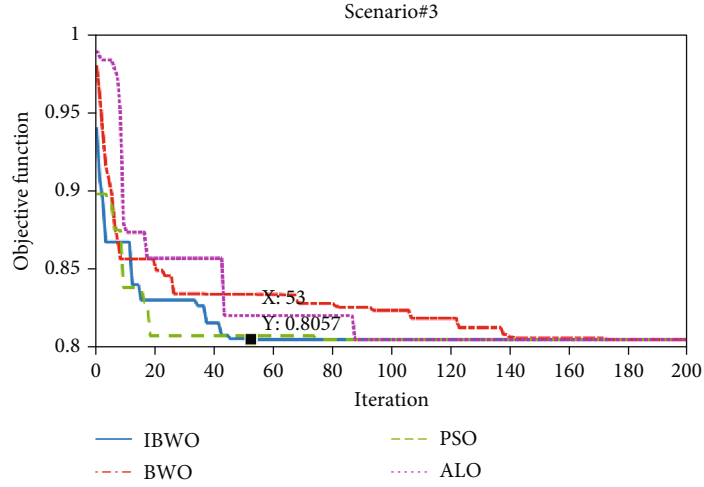

Figure 12: Convergence process of different methods for scenario 3.

Table 6: Numerical results of scenario 3 (Recon) using different optimization methods.

	Base net	IBWO	BWO	PSO	ALO
Opened switches	33, 34, 35, 36, 37	7, 10, 14, 28, 32	7, 10, 14, 28, 32	7, 10, 14, 28, 32	7, 10, 14, 28, 32
Power losses (kW)	1824.79	1283.77	1283.77	1283.77	1283.77
ENS (MWh/yr)	53.930	43.84	43.84	43.84	43.84
SAIFI (failure/customer/yr)	4.10	3.38	3.38	3.38	3.38
SAIDI (hour/customer/yr)	48.65	42.89	42.89	42.89	42.89
OF	—	0.8056	0.8056	0.8056	0.8056

WT, and battery numbers are determined as 149, 381, and 570, respectively. Based on the decision variables determined by the IBWO, the energy losses, ENS, SAIFI, SAIDI, and HMG cost are obtained at 613.29 kWh, 24.81 MWh, 2.04, 32.30, and $148,625.48, respectively. The results obtained from different methods show that each of the methods has achieved an optimal network configuration different from the other and also provided the installation location and different capacities of the HMGs. The results of proposed methodology based on the hybrid multi-microgrid allocation and network reconfiguration are demonstrated that the losses, ENS, SAIDI, and SAIFI are reduced by 66.39%, 54.00%, 50.24%, and 33.61%, respectively, for 33-bus network in comparison with the base network. The comparison of the results, like the previous scenarios, shows the better performance of the IBWO method in further improving

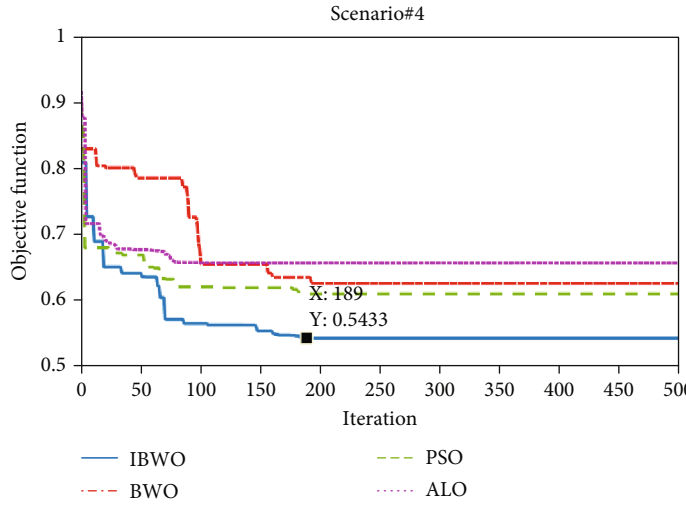

Figure 13: Convergence process of different methods for scenario 4.

Table 7: Numerical results of scenario 4 (Recon+one HMG) using different optimization methods.

	Base net	IBWO	BWO	PSO	ALO
HS_1 location (bus)	—	@ 17	@ 10	@ 29	@ 9
PV_1 size (kW)	—	12	54	383	246
WT_1 size (kW)	—	156	306	302	417
$Battery_1$ size (kWh)	—	80	137	433	2476
Opened switches	—	7, 10, 14, 16, 28	7, 8, 9, 28, 31	7, 9, 14, 27, 32	4, 11, 14, 17, 28
Power losses (kW)	1824.79	1150.46	1157.20	1006.61	1228.82
ENS (MWh/yr)	53.93	37.94	34.69	32.21	26.51
SAIFI (failure/customer/yr)	4.10	2.07	3.22	3.05	3.09
SAIDI (hour/customer/yr)	48.65	32.42	41.63	40.29	40.62
HMG cost ($)	—	42,019.63	79655.30	81537.07	113247.62
OF	—	0.5432	0.6261	0.6099	0.6569

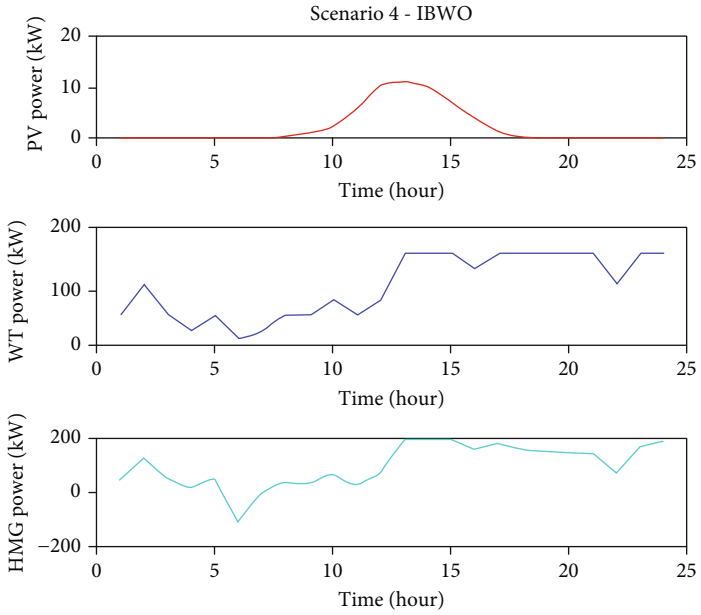

Figure 14: Contribution of the different HMG components for scenario 4.

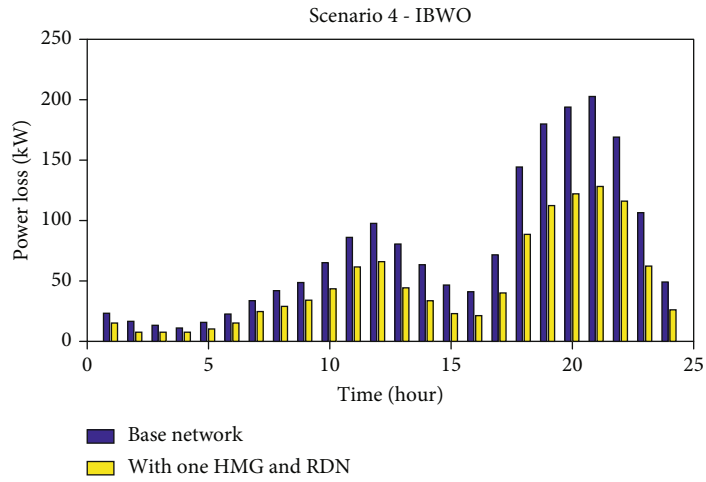

Figure 15: Power loss of the 33-bus network using the IBWO for scenario 4.

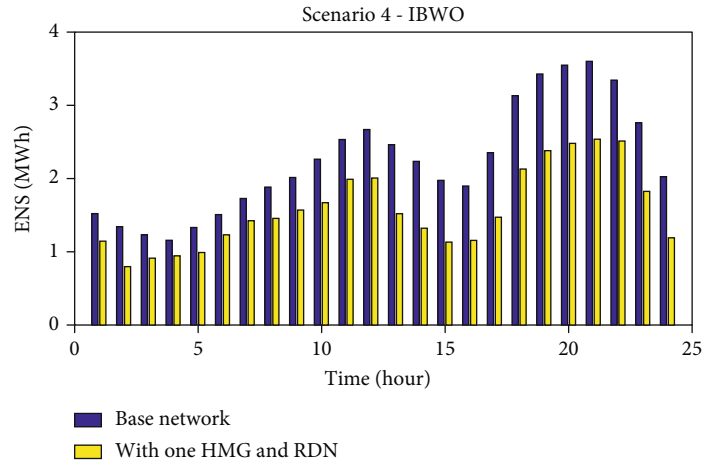

Figure 16: ENS of the 33-bus network using the IBWO for scenario 4.

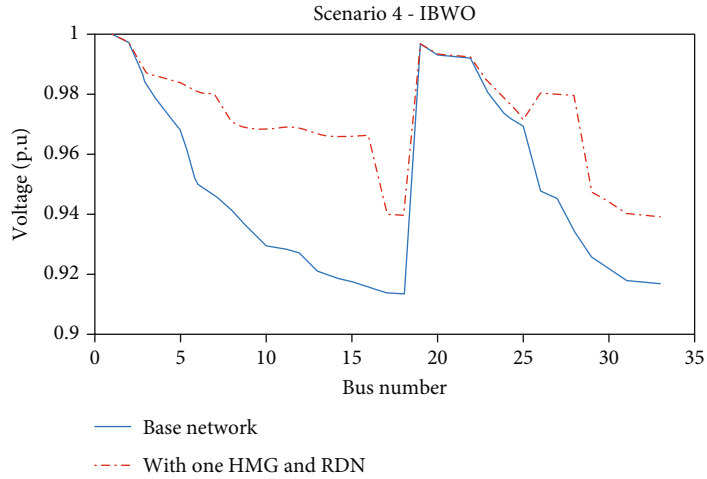

Figure 17: Voltage profile of the 33-bus network using the IBWO for scenario 4.

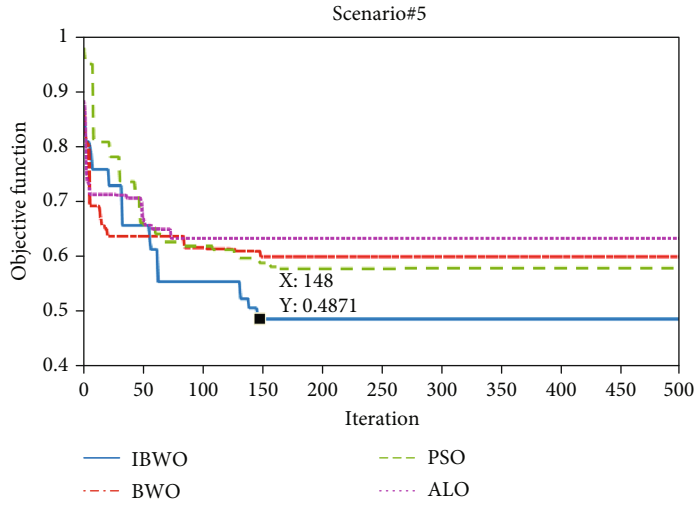

Figure 18: Convergence process of different methods for scenario 5.

Table 8: Numerical results of scenario 5 (Recon+two HMGs) using different optimization methods.

	Base net	IBWO	BWO	PSO	ALO
HS_1 location (bus)	—	@ 33	@ 23	@ 28	@ 9
PV_1 size (kW)	—	14	65	130	224
WT_1 size (kW)	—	174	214	212	290
$Battery_1$ size (kWh)	—	22	53	315	652
HS_2 location (bus)	—	@ 17	@ 33	@ 10	@ 29
PV_2 size (kW)	—	149	381	313	291
WT_2 size (kW)	—	381	461	306	161
$Battery_2$ size (kWh)	—	570	2654	1604	833
Opened switches	—	7, 10, 14, 16, 28	7, 11, 14, 17, 22	7, 9, 14, 17, 26	9, 14, 13, 25, 31
Power losses (kW)	1824.79	613.29	1059.26	1028.01	1266.95
ENS (MWh/yr)	53.93	24.81	32.49	28.45	31.97
SAIFI (failure/customer/yr)	4.10	2.04	2.66	2.89	3.36
SAIDI (hour/customer/yr)	48.65	32.30	37.15	38.96	42.76
HMG cost ($)		148,625.48	180,984.21	140,382.21	121,799.82
OF	—	0.4871	0.6000	0.5794	0.6335

various goals, including reducing energy losses and improving reliability indicators.

In Figure 19, the power variation curve of PV and WT sources, as well as the injected power of HMG related to both HMGs to the network, is depicted. The HMG system with battery storage charge and discharge management has been able to inject continuous and planned power into the distribution network. The battery storage system stores excess power over the load's needs and discharges the stored energy to supply the network load in times of power shortage of renewable resources to supply the load with a high level of resilience.

In Figures 20 and 21, the curve of changes in network power losses as well as changes in ENS is shown before and after the scheduling of two HMGs and network reconfiguration during 24 hours. In scenario 5, in all hours, network power losses, especially peak load, based on the planned injection of HMG power, as well as network reconfiguration and network power flow path changes, have declined from 1824.79 kWh, energy loss in the base network to 613.29 kWh. Also, in Figure 21, the ENS of the network subscribers has decreased in all hours, which is an effective problem of battery reserve power management in the HMG system, thus enhancing the reliability of the network and reducing the value of ENS from 53.93 MWh to 24.81 MWh.

Figure 22 also shows the voltage profile curve of the 33-bus network before and after the scheduling of two HMGs and the network reconfiguration, which is found to have improved significantly network voltage profile.

5.1.6. The Results of Scenario Comparison, 33-Bus Network. This section compares the efficacy of various scenarios in Table 9. The scenario with the lowest value of the objective function (see Figure 23), as well as the quantity of energy loss, ENS, SAIFI, and SAIDI, has the greatest efficiency, as can be seen in scenario 5. Scenario 5 is able to further enhance the

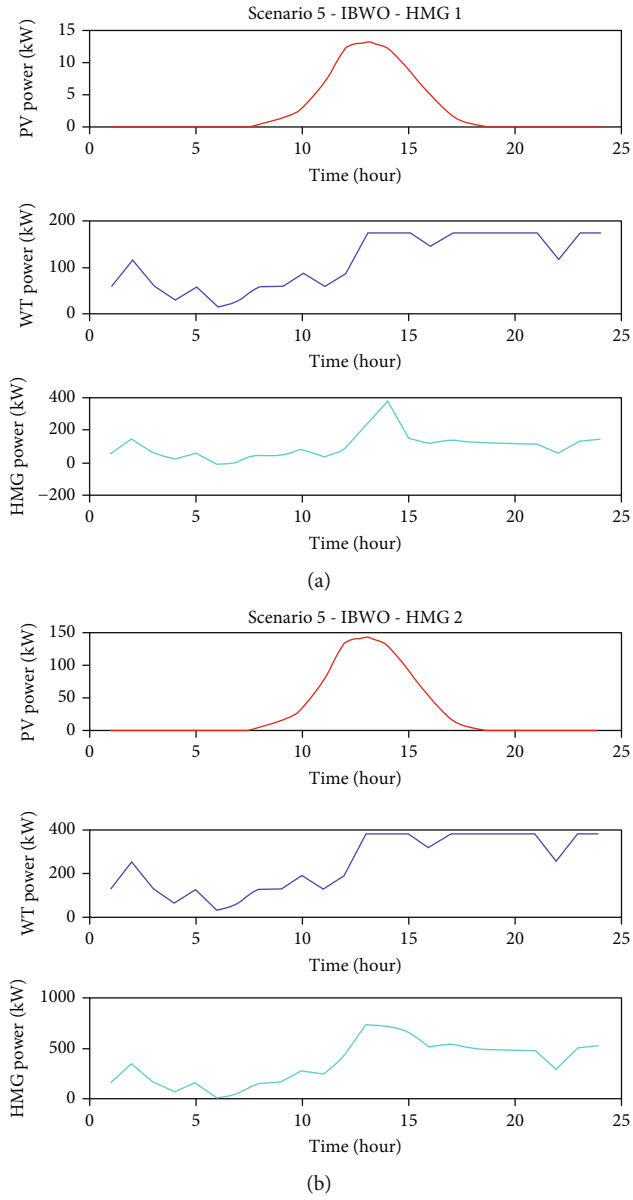

Figure 19: Contribution of the different HMG components in 33-bus network for scenario 5: (a) first HMG; (b) second HMG.

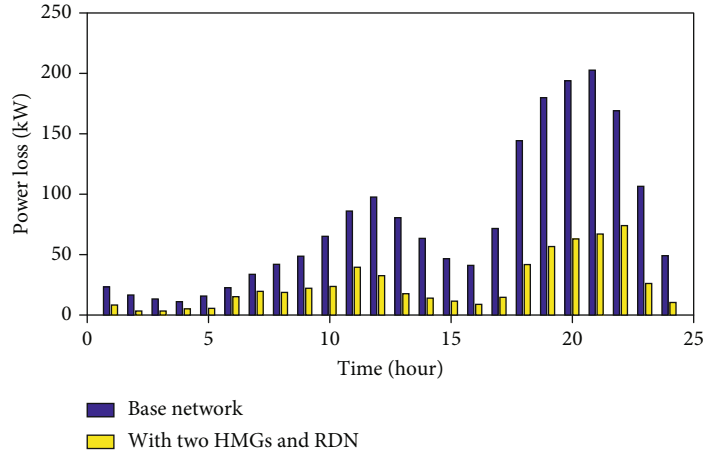

Figure 20: Power loss of the 33-bus network using the IBWO for scenario 5.

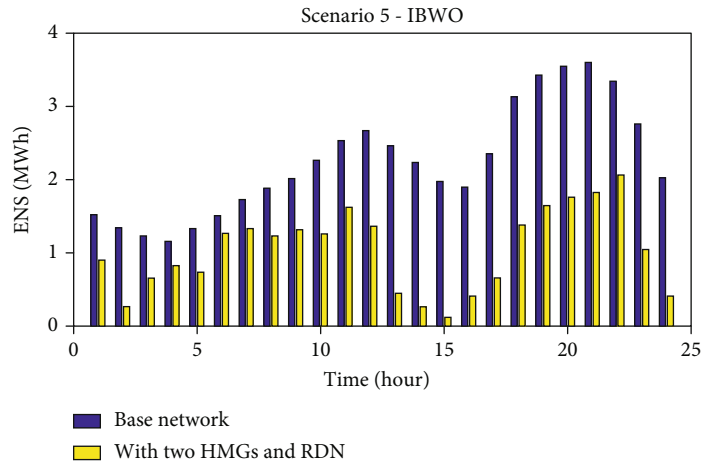

Figure 21: ENS of the 33-bus network using the IBWO for scenario 5.

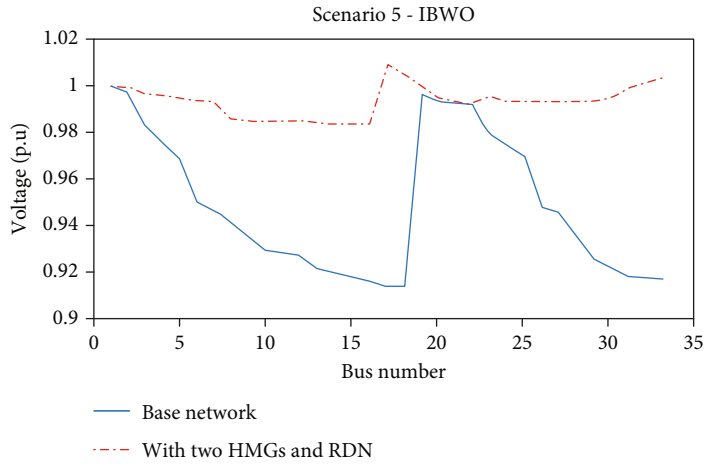

Figure 22: Voltage profile of the 33-bus network using the IBWO for scenario 5.

Table 9: The numerical result comparison of different scenarios using the IBWO for 33-bus network.

	Base net	Scenario #1	Scenario #2	Scenario #3	Scenario #4	Scenario #5
HS_1 location (bus)	—	Bus 33	Bus 33	—	Bus 17	Bus 33
PV_1 size (kW)	—	2	1	—	12	14
WT_1 size (kW)	—	252	180	—	156	174
$Battery_1$ size (kWh)	—	17	75	—	80	22
HS_2 location (Bus)	—	—	Bus 15	—	—	@ 17
PV_2 size (kW)	—	—	284	—	—	149
WT_2 size (kW)	—	—	394	—	—	381
$Battery_2$ size (kWh)	—	—	570	—	—	570
Opened switches	—	33, 34, 35, 36, 37	33, 34, 35, 36, 37	7, 10, 14, 28, 32	7, 10, 14, 16, 28	7, 10, 14, 16, 28
Power losses (kW)	1824.79	1275.12	963.06	1283.77	1150.46	613.29
ENS (MWh/yr)	53.93	44.77	27.58	43.84	37.94	24.81
SAIFI (failure/customer/yr)	4.10	2.06	2.75	3.38	2.07	2.04
SAIDI (hour/customer/yr)	48.65	32.36	37.84	42.89	32.42	32.30
HMG cost ($)		65,576.17	155,445.61	—	42019.63	148625.48
OF	—	0.5910	0.5559	0.8056	0.5432	0.4870

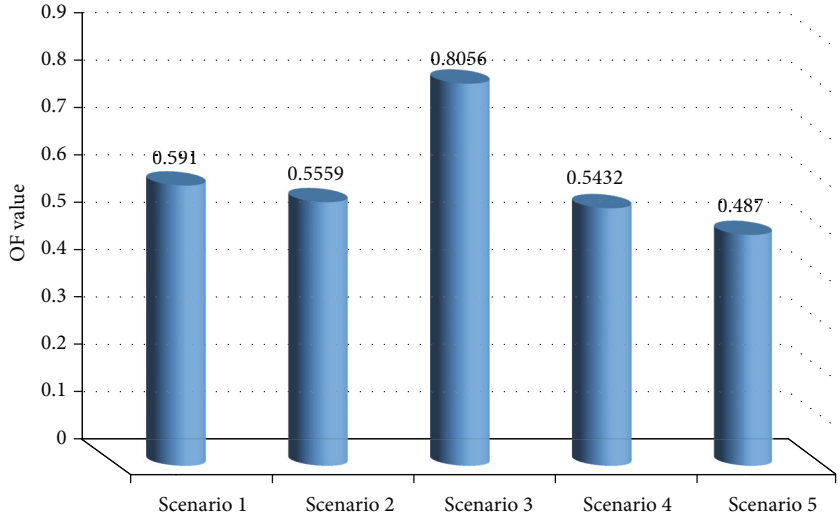

Figure 23: Comparison of the fitness function in the scenarios for 33-bus network.

Table 10: Numerical results of scenario 6 (Recon+two HMGs) considering SH using IBWO.

	Base net	Without SH	With SH (L18)	With SH (L22)	With SH (L25)
HS_1 location (bus)	—	@ 33	@ 17	@ 16	@ 13
PV_1 size (kW)	—	14	1	119	3
WT_1 size (kW)	—	174	193	219	192
$Battery_1$ size (kWh)	—	22	34	349	115
HS_2 location (bus)	—	@ 17	@ 28	@ 23	@ 27
PV_2 size (kW)	—	149	220	220	68
WT_2 size (kW)	—	381	489	486	500
$Battery_2$ size (kWh)	—	570	1625	1664	988
Opened switches	—	7, 10, 14, 16, 28	12, 21, 27, 36	6, 9, 13, 32	7, 9, 12, 36
Power losses (kW)	1824.79	613.29	1117.93	1093.44	626.49
ENS (MWh/yr)	53.930	24.819	33.745	33.010	25.005
SAIFI (failure/customer/yr)	4.10	2.04	3.20	3.74	2.24
SAIDI (hour/customer/yr)	48.65	32.30	40.07	43.64	33.76
HMG cost ($)	—	148625.48	183149.31	191177.52	187740.62
OF	—	0.4870	0.5870	0.6409	0.4994

network's efficiency by identifying the optimal configuration of the 33-bus network by opening switches 7, 10, 14, 16, and 28 and placing two HMGs in buses 33 and 17. Scenario 3 with network reconfiguration has seen the least improvement over time. Upon analyzing the results, it is determined that the incorporation of network reconfiguration with HMG or HMG scheduling (comparing scenarios 1 and 4 and scenarios 2 and 5) enhanced each of the objectives.

5.2. The Simulation Results with SH

5.2.1. The Simulation Results with SH for 33-Bus Network. The numerical results of the operation of a 33-bus distribution network based on two HMG scheduling and the network reconfiguration are given considering SH (scenario 6) using the IBWO algorithm in Table 10. The performance of scenario 6 in SH conditions with the occurrence of a fault in lines 18, 22, and 25 of the network in hour 1:00 of simulation has been investigated. The results demonstrated that in the event of a fault in any of the lines, during 24 hours, disconnecting and connecting the network switches to obtain the optimum configuration of the network and also the scheduling of HMGs was done in such a way that in addition to minimizing network energy losses and the cost of energy injection of HMGs into the network, resilience indicators such as ENS, SAIFI, and SAIDI are minimized to provide better self-healing. According to Table 10, it is observed that in the event of a fault in each of lines 18, 22, and 25 of the network, the recommended method integrates the optimal scheduling of HMGs well by determining the optimal configuration of the network with the open and closed switches of the network, and thus, it has improved reliability and self-healing. Also, the results demonstrated that the costs of HMG energy generation and power

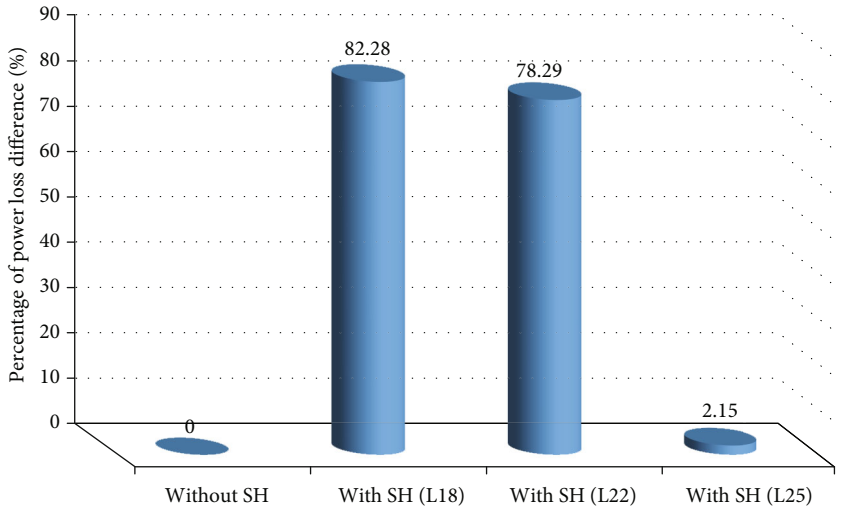

Figure 24: Increasing percentage of the power loss considering line outage of 33-bus network for scenario 6.

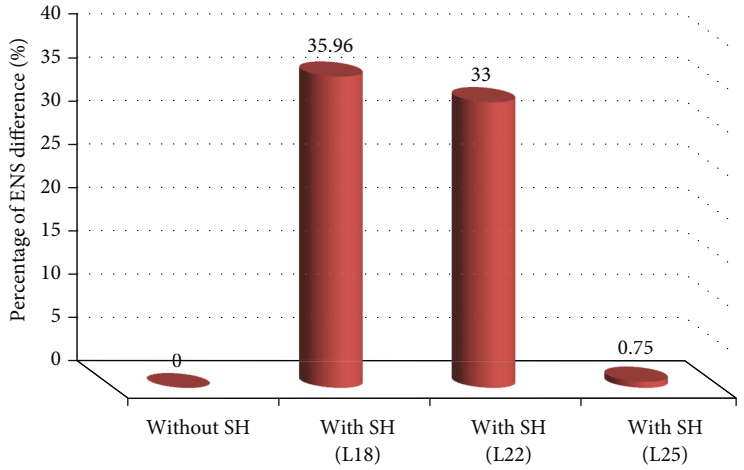

Figure 25: Increasing percentage of the ENS considering line outage of 33-bus network for scenario 6.

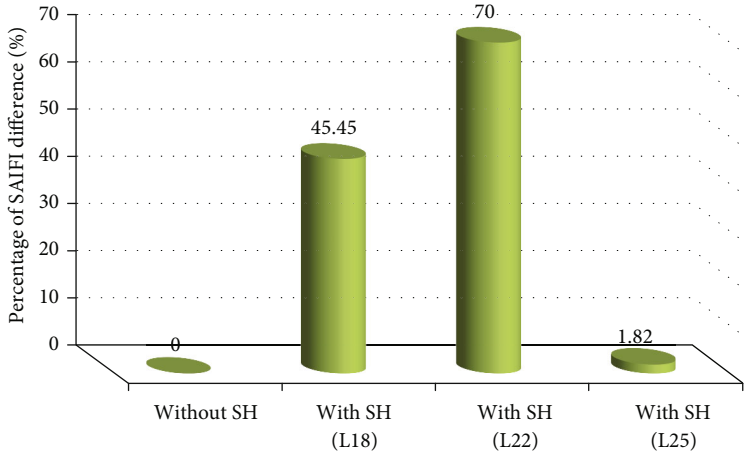

Figure 26: Increasing percentage of the SAIFI considering line outage of 33-bus network for scenario 6.

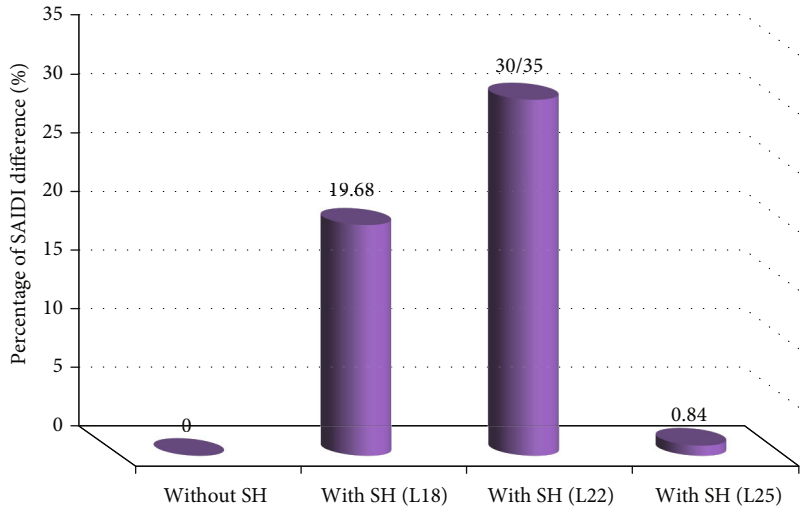

Figure 27: Increasing percentage of the SAIDI considering line outage of 33-bus network for scenario 6.

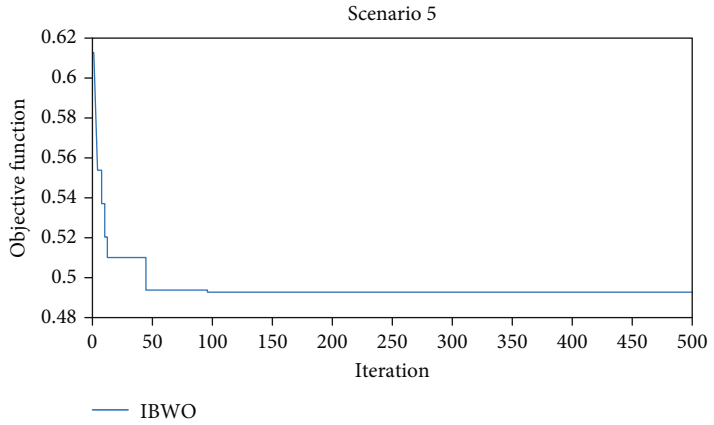

Figure 28: Convergence process of IBWO in 59-bus network for scenario 5.

Table 11: Numerical results of scenario #5 (Recon+two HMGs) using IBWO for real 59-bus network.

Item/value	Base net	Without SH (base scenario 5)
HS_1 location (bus)	—	@ 33
PV_1 size (kW)	—	69
WT_1 size (kW)	—	356
$Battery_1$ size (kWh)	—	122
HS_2 location (bus)	—	@ 28
PV_2 size (kW)	—	744
WT_2 size (kW)	—	428
$Battery_2$ size (kWh)	—	897
Opened switches	—	19, 29, 32, 53, 62
Power losses (kW)	1651.23	573.12
ENS (MWh/yr)	346.178	147.320
SAIFI (failure/customer/yr)	8.74	4.49
SAIDI (hour/customer/yr)	85.75	32.30
HMG cost ($)	—	148,625.48
OF	—	0.4927

injection to the network have increased compared to the conditions before the fault occurred in different lines.

The percentage changes of each of the goals compared to the base value in scenario 6, considering SH per fault occurrence in different network lines, are shown in Figures 24–27. Based on Figures 24 and 25, the highest deviation of energy losses and ENS is related to the fault occurrence in line 18 and the lowest value is related to line 25. Also, according to Figures 26 and 27, the highest deviation of SAIFI and SAIDI is related to the occurrence of fault in line 22 and its lowest value is related to line 25. In comparison to scenario 5 without the line outages, the findings revealed that the network loss increased by 82.28% ((1117.93-613.29)/613.29∗100) and 2.15% ((626.49-613.29)/613.29∗100)), respectively, when lines 18 and 25 are faulted. Furthermore, when lines are unavailable, the ENS, SAIFI, and SAIDI increased by 26.45%, 56.86%, and 24.06% and by 0.75%, 9.80%, and 4.52%, respectively, when compared to scenario 5 without line outages.

5.2.2. The Simulation Results with SH for Real 59-Bus Network. The outcomes of applying the IBWO algorithm to a 59-bus distribution network with HMG scheduling

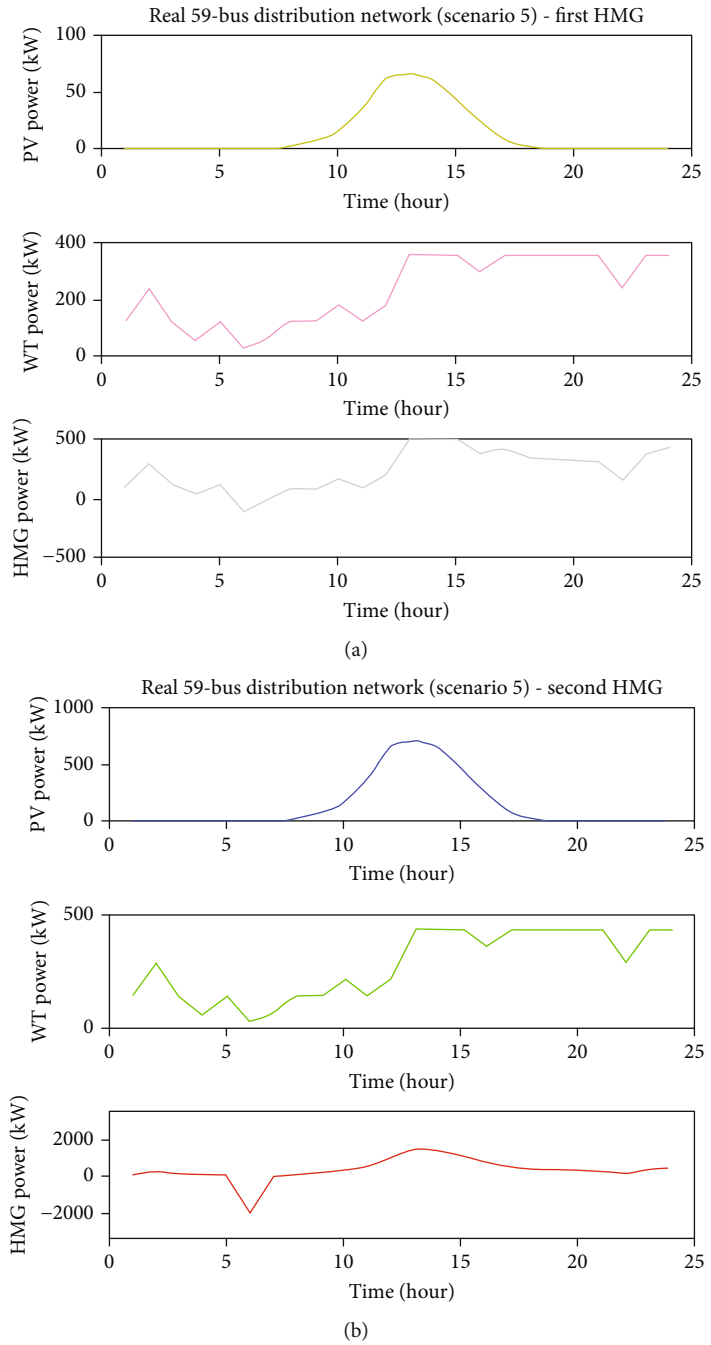

Figure 29: Contribution of the different HMG components in 59-bus network for scenario 5: (a) first HMG; (b) second HMG.

and no SH consideration are provided. Convergence process of IBWO for 59-bus network to solve the scenario 5 using the IBWO is depicted in Figure 28. The numerical results of the implementation of scenario 5 on the 59-bus network using the IBWO algorithm are given in Table 11. It can be seen that with the optimal allocation and scheduling of two HMGs in buses 33 and 28 of the network and by opening lines 19, 29, 32, 53, and 62, the power loss has decreased from 1,651.23 kW to 573.12 kW. Also, the ENS, SAIFI, and SAIDI reliability indices are obtained 147.320 MWh, 4.49 failure/customer/yr, and 32.30 hour/customer/yr, respectively, which are significantly improved. Therefore, using two HMGs has reduced power losses, ENS, SAIFI, and SAIDI by 65.29%, 57.44%, 48.63%, and 62.33%, respectively, in comparison with the basic network without reconfiguration and also HMG allocation. The results are given that the losses, ENS, SAIDI, and SAIFI are declined by 65.29%, 57.44%, 48.63%, and 62.33%, respectively, for the real 59-bus Ahvaz network in comparison with the base network.

The power variations of the PV and WT sources, along with the injected power of the HMG associated with both HMGs to the 59-bus network for scenario 5, are shown in Figure 29. Constant and scheduled power injection into the distribution network has been made possible by the HMG

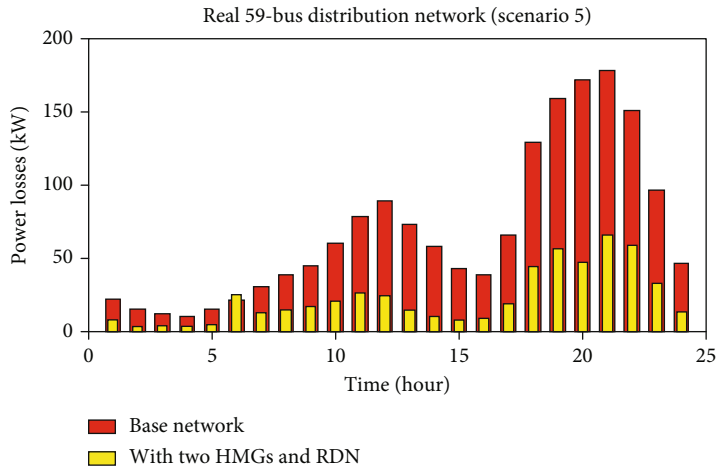

Figure 30: Power loss of the 59-bus network using the IBWO for scenario 5.

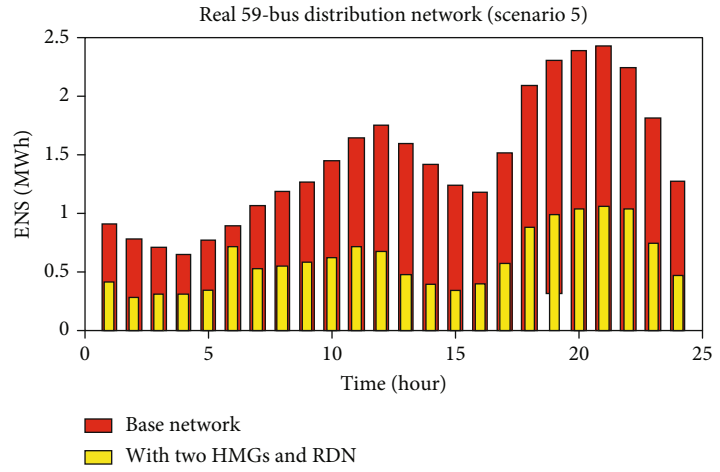

Figure 31: ENS of the 59-bus network using the IBWO for scenario 5.

Table 12: Numerical results of scenario 6 (Recon+two HMGs) considering SH using IBWO for real 59-bus network.

	Base net	Without SH (base scenario 5)	With SH (L12)	With SH (L14)
HS_1 location (bus)	—	@ 33	@ 34	@ 15
PV_1 size (kW)	—	69	518	4
WT_1 size (kW)	—	356	373	291
$Battery_1$ size (kWh)	—	122	255	288
HS_2 location (bus)	—	@ 28	@ 28	@ 33
PV_2 size (kW)	—	744	503	813
WT_2 size (kW)	—	428	304	348
$Battery_2$ size (kWh)	—	897	111	315
Opened switches	—	19, 29, 32, 53, 62	24, 30, 37, 51	25, 32, 34, 40
Power losses (kW)	1651.23	573.12	872.97	1017.83
ENS (MWh/yr)	346.178	147.320	162.487	159.702
SAIFI (failure/customer/yr)	8.74	4.49	5.94	4.63
SAIDI (hour/customer/yr)	85.75	32.30	58.03	38.13
HMG cost ($)	—	148625.48	184416.39	169763.00
OF	—	0.4927	0.6068	0.5460

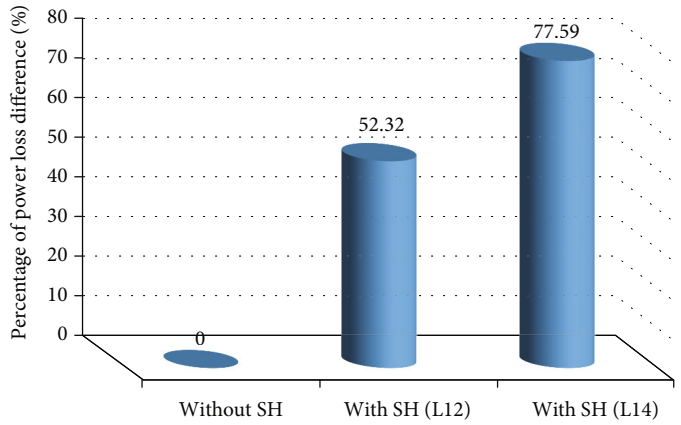

Figure 32: Increasing percentage of the power loss considering line outage of 59-bus network for scenario 6.

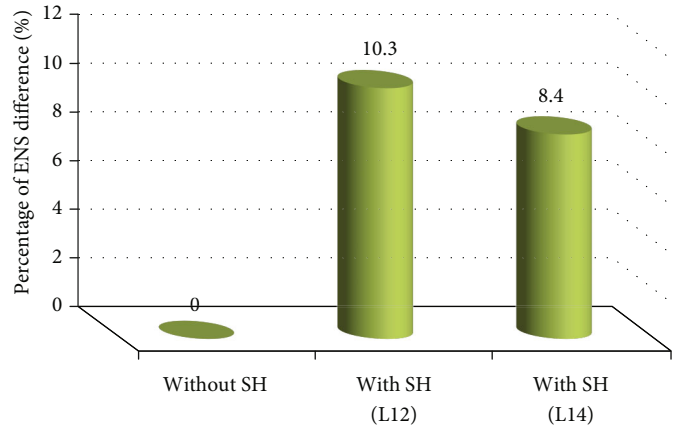

Figure 33: Increasing percentage of the ENS considering line outage of 59-bus network for scenario 6.

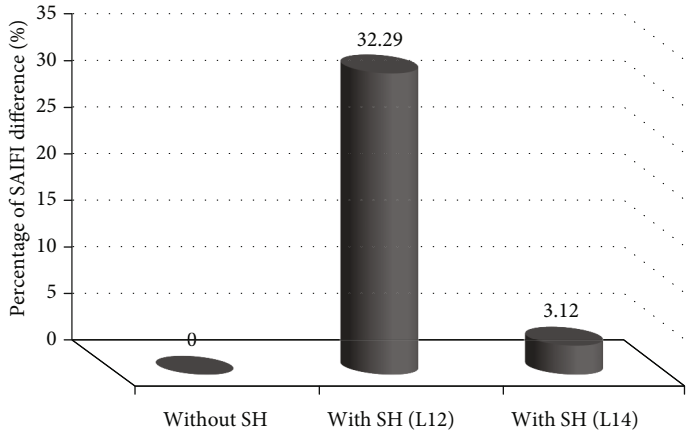

Figure 34: Increasing percentage of the SAIFI considering line outage of 59-bus network for scenario 6.

system with battery storage charge and discharge management. When there is a power deficit of renewable resources, the battery storage system releases its stored energy to supply the network load with a high degree of reliability. It also stores excess power beyond the needs of the load.

Before and after the scheduling of two HMGs and network reconfiguration over a 24 hours period, the curves of changes in network power losses and ENS are depicted in Figures 30 and 31, respectively. The power losses have been reduced from 1651.23 kWh to 573.12 kWh in scenario 5. This reduction is the result of the intended injection of HMG power, network reconfiguration, and changes in the power flow path of the network. Additionally, the ENS of the network subscribers has exhibited a consistent decrease throughout the day, as depicted in Figure 31. This diminishing value of ENS from 346.178 MWh to 147.320 MWh

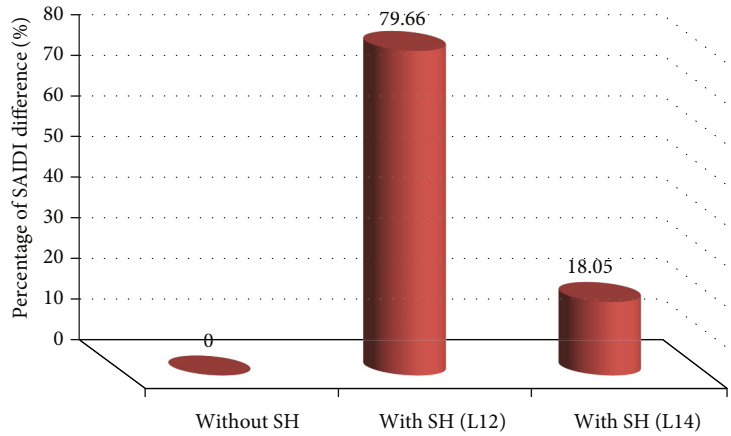

Figure 35: Increasing percentage of the SAIDI considering line outage of 59-bus network for scenario 6.

effectively addresses an issue with battery reserve power management in the HMG system, thereby bolstering the network's reliability.

The numerical results of the 59-bus network's operation in accordance with HMG scheduling and network reconfiguration (scenario 6) taking into account the SH via the IBWO are presented in Table 12. The efficiency of scenario 6 under SH conditions, including disruptions on lines 12 and 14, was assessed during hour 1:00 of the simulations. The findings indicated that, should a malfunction occur in these critical lines, the process of reconnecting and disabling network switches to attain the most efficient network configuration, in conjunction with HMG scheduling, reduces network energy losses and expenses associated with HMG energy injection. This, in turn, aids in the enhancement of self-healing capabilities by decreasing reliability metrics including ENS, SAIFI, and SAIDI. The proposed method integrates the optimal scheduling of HMG, as shown in Table 12. This is achieved by determining the optimal network configuration using the open and closed switches of the network. As a result, the proposed method ensures improved reliability and self-healing capabilities in the event that a fault occurs in lines 12 and 14. Furthermore, the findings unveiled that the expenses associated with microgrids, energy generation, and power injection into the grid have escalated in comparison to the conditions that prevailed prior to the occurrence of multiple line faults.

The results showed that with the outage of lines 12 and 14, respectively, the network loss increased by 52.32% ((872.97-573.12)/573.12∗100) and 77.59% ((1017.83-573.12)/573.12∗100) compared to the scenario 5 without the outage of lines. Moreover, considering the outage of line 12, the ENS, SAIFI, and SAIDI are increased 10.30%, 32.29%, and 79.66%, and also considering the outage of line 14, these objectives are increased by 8.40%, 3.12%, and 18.05%, respectively, compared with the scenario 5 without any outages (see Figures 32–35). By examining the results presented in Table 12 and Figures 32–35, it can be seen that the network loss with the outage of line 14 is higher compared to the condition of the outage of line 12. On the other hand, the results confirm that the outage of line 12 has further weakened the network reliability compared with the outage of line 14.

6. Conclusion

This study proposed the 33- and 59-bus distribution network operation by employing simultaneous scheduling of multi-HMGs integrated with a reconfiguration for reliability improvement considering self-healing in fault occurrence in the network lines for minimizing the energy losses, cost of the multi-HMGs, ENS, SAIDI, and SAIFI indices during 24 hours of the study horizon. The IBWO was applied to find the decision variable to minimize the multi-objective function and satisfy the operational and multi-HMG constraints. Seven scenarios were considered to evaluate the effectiveness of the proposed method including scheduling of one microgrid, two microgrids, network reconfiguration, simultaneous scheduling of one HMG with reconfiguration, and simultaneous scheduling of two HMGs with reconfiguration, and also, the last two scenarios were implemented along with self-healing. The findings of the study were summarized as follows:

(i) The simulation results showed that the scheduling scenario of two microgrids with reconfiguration in the condition without self-healing had the highest performance improvement. In other words, the greatest reduction in energy losses and reliability indicators is related to this scenario, and the weakest performance was related to the reconfiguration-only scenario

(ii) The results of HMG scheduling showed that the battery storage system, by compensating the power fluctuations of renewable energy sources with charge and discharge energy management, was able to inject programmable power into the distribution network, thereby improving the network performance and reliability indices

(iii) The simulation results have confirmed that by optimally changing the status of network switches in the event of a fault, the network can be self-healing, and with optimal HMG scheduling, various network objectives, especially resilience, had improved significantly compared to the basic network

(iv) The results demonstrated the superiority of the proposed IBWO compared to other algorithms and had led to lower energy losses and higher reliability improvement. It was also found that improving the capability of the conventional BWO with the nonlinearly diminishing inertia weight approach had improved its exploration power and increased the speed and accuracy of its convergence in reaching the optimal global solution

(v) The findings indicated that self-healing is achieved in the event of network line outages through the concurrent implementation of reconfiguration, allocation, and optimal scheduling of HMGs in the distribution network. As a result, reliability indices have improved while energy losses and the cost of injecting energy into the network via HMGs have been reduced

(vi) The findings from the suggested approach, which combines hybrid multi-microgrid placement and network reconfiguration, show significant improvements, specifically, losses, ENS, SAIDI, and SAIFI decreased by 66.39%, 54.00%, 50.24%, and 33.61%, respectively, for a 33-bus network, and saw reductions of 65.29%, 57.44%, 48.63%, and 62.33%, respectively, for the actual 59-bus Ahvaz network when compared to the base network

(vii) The results showed that with the outage of lines 12 and 14 of the 33-bus network in scenario 5, respectively, the network loss is increased by 82.28% and 2.15%, the ENS is increased by 26.45% and 0.75%, the SAIFI is increased by 56.86% and 9.80%, and the SAIDI is raised by 24.06% and 4.52% compared with the scenario 5 without any outages

(viii) The results showed that with the outage of lines 12 and 14 of the real 59-bus network in scenario 5, respectively, the network loss is increased by 52.32% and 77.59%, the ENS is increased by 10.30% and 8.40%, the SAIFI is increased by 32.29% and 3.12%, and the SAIDI is raised by 79.66% and 18.05% compared with the scenario 5 without any outages

(ix) Distribution network operation based on multi-microgrids and multi-storage scheduling and reconfiguration to enhance the reliability considering self-healing incorporating uncertainty is suggested for future work

Nomenclature

C_{BA}: Purchase cost of each battery
$C_{BA,OP\&M}$: Annual maintenance cost of batteries
C_{INV}: Purchase cost of each inverter
$C_{OP\&M}$: Annual maintenance and operation cost
C_{PV}: Purchase cost of each PV
$C_{PV,OP\&M}$: Annual maintenance cost of PV
Cu_k: Current passing through the line k
Cu^i_{max}: Upper current passing through the line i
C_{WT}: Purchase cost of each WT
$C_{WT,OP\&M}$: Annual maintenance cost of WT
DLR_i: Duration of line i repair
DOD: Depth of discharge
$E_{BA}(t)$: Battery energy values at hours t
$E^{min}_{BA}, E^{max}_{BA}$: Lower and upper energy limit of the battery
ENS^T_{NET}: Total network energy not-supplied
LL_i: Length of line i
N_i: Number of subscribers at load point i
n_{BA}: Number of batteries
n_{INV}: Inverter efficiency
NLL: Number of lost loads due to line outage
NPC_{HMG}: Net present cost of the HMG
n_{PV}: Number of PVs
$n^{min}_{PV}, n^{max}_{PV}$: Minimum and upper number of PVs
$n^{min}_{WT}, n^{max}_{WT}$: Minimum and upper number of WTs
n_{WT}: Number of WTs
P_{BA-INV}: Battery power injected to the inverter
P_{Dmd}: Active load of the network
P_{Dmd}: Active load of the network
P_{HMG}: Active power transferred from the hybrid system into the grid
$P_{Inv-Load}$: Transferred power from the inverter to the load
P^T_L: Total active power loss
P_{NET}: The network load power
P_{Post}: Active post power
P_{PV}: Power of PV
P^T_{PV}: Total power of PV
$P_{PV-Rated}$: Rated power of PV
$P_{RES-INV}$: Renewable energy sources power transmitted to the inverter
P_{WT}: Power of WT
P^T_{WT}: Total power of WT
$P_{WT-Rated}$: Rated power of WT
Q_{Dmd}: Reactive load of the network
Q_{HMG}: Reactive power transferred from the hybrid system into the grid
Q_{Post}: Reactive post power
RES_k: Ohmic resistance of the line k
RLO_i: Rate of line i outage
SAIDI: System average interruption duration index
SAIFI: System average interruption frequency index
TEM_C: Temperature of the PV cell
TEM_R: Temperature of the PV in the reference condition
VOL_i: Voltage of buses i
VOL_j: Voltage of buses j
VOL^i_{max}: Upper value of the bus i voltage
VOL^i_{min}: Lower value of the bus i voltage
W_f: Whale stranding
WS: Wind speed
WS_{Cut-in}: Cut-in wind speed
$WS_{Cut-out}$: Cut-out wind speed
WS_{Rated}: Rated wind speed
X_{step}: Step dimension of whale descent

X_i^T: Resent location of the ith beluga whale
$X_{i,j}^{T+1}$: New positioning of the ith beluga whale in the j th dimension
$X_{i,pj}^T$: Current coordinates of the ith beluga whales
X_r^T: Current situation of an arbitrary beluga whale
$X_{r,p1}^T$: Current coordinates of the rth beluga whales
φ: Weighting coefficient
ϖ: Self-discharge
λ_i: Failure rate of load points i
γ_{BA}: Battery charging yield
ρ_i: Lost load due to line i outage
∂: Radiation perpendicular to the PV surface
∂_{Ref}: Standard test condition radiation
γ_{TC}: Temperature coefficient of the PV panel.

Data Availability

The data applied to support the research outcomes are given within the paper (Table 3) and also Ref. [31].

Conflicts of Interest

The authors declare that they have no conflicts of interest.

Authors' Contributions

Alireza Kalantari was responsible for the conceptualization, methodology, and software and wrote the original draft. Hamid Lesani was responsible for the supervision, investigation, and validation and wrote, reviewed, and edited the manuscript.

References

[1] A. Naderipour, S. A. Nowdeh, P. B. Saftjani et al., "Deterministic and probabilistic multi-objective placement and sizing of wind renewable energy sources using improved spotted hyena optimizer," *Journal of Cleaner Production*, vol. 286, article 124941, 2021.

[2] M. Ghanbari-Ghalehjoughi, K. Taghizad-Tavana, and S. Nojavan, "Resilient operation of the renewable energy and battery energy storages based smart distribution grid considering physical-cyber-attacks," *Journal of Energy Storage*, vol. 62, article 106950, 2023.

[3] M. Yadav, N. Pal, and D. K. Saini, "Low voltage ride through capability for resilient electrical distribution system integrated with renewable energy resources," *Energy Reports*, vol. 9, pp. 833–858, 2023.

[4] S. A. Nowdeh, A. Naderipour, I. F. Davoudkhani, and J. M. Guerrero, "Stochastic optimization–based economic design for a hybrid sustainable system of wind turbine, combined heat, and power generation, and electric and thermal storages considering uncertainty: a case study of Espoo, Finland," *Renewable and Sustainable Energy Reviews*, vol. 183, article 113440, 2023.

[5] M. Shirkhani, J. Tavoosi, S. Danyali et al., "A review on microgrid decentralized energy/voltage control structures and methods," *Energy Reports*, vol. 10, pp. 368–380, 2023.

[6] L. Pan, F. Wang, Y. He et al., "Reassessing self-healing in metallized film capacitors: a focus on safety and damage analysis," *IEEE Transactions on Dielectrics and Electrical Insulation*, vol. 31, 2024.

[7] A. F. Shahsavari, S. M. Mazhari, and H. Lesani, "A joint automatic and manual switch placement within distribution systems considering operational probabilities of control sequences," *International Transactions on Electrical Energy Systems*, vol. 25, no. 11, pp. 2745–2768, 2015.

[8] Ž. Popović, B. Brbaklić, and S. Knežević, "A mixed integer linear programming based approach for optimal placement of different types of automation devices in distribution networks," *Electric Power Systems Research*, vol. 148, pp. 136–146, 2017.

[9] S. M. Mohammadi-Hosseininejad, A. Fereidunian, A. Shahsavari, and H. Lesani, "A healer reinforcement approach to self-healing in smart grid by PHEVs parking lot allocation," *IEEE Transactions on Industrial Informatics*, vol. 12, no. 6, pp. 2020–2030, 2016.

[10] M. Rahmani-Andebili, "Distributed generation placement planning modeling feeder's failure rate and customer's load type," *IEEE Transactions on Industrial Electronics*, vol. 63, no. 3, pp. 1598–1606, 2016.

[11] G. Ferro, F. Laureri, R. Minciardi, and M. Robba, "An optimization model for electrical vehicles scheduling in a smart grid," *Sustainable Energy, Grids and Networks*, vol. 14, pp. 62–70, 2018.

[12] A. Fathy and A. Y. Abdelaziz, "Competition over resource optimization algorithm for optimal allocating and sizing parking lots in radial distribution network," *Journal of Cleaner Production*, vol. 264, article 121397, 2020.

[13] M. M. Landi, M. Mohammadi, and M. Rastegar, "Simultaneous determination of optimal capacity and charging profile of plug-in electric vehicle parking lots in distribution systems," *Energy*, vol. 158, pp. 504–511, 2018.

[14] D. L. Duan, X. D. Ling, X. Y. Wu, and B. Zhong, "Reconfiguration of distribution network for loss reduction and reliability improvement based on an enhanced genetic algorithm," *International Journal of Electrical Power & Energy Systems*, vol. 64, pp. 88–95, 2015.

[15] A. Jafari, H. G. Ganjehlou, F. B. Darbandi, B. Mohammadi-Ivatloo, and M. Abapour, "Dynamic and multi-objective reconfiguration of distribution network using a novel hybrid algorithm with parallel processing capability," *Applied Soft Computing*, vol. 90, article 106146, 2020.

[16] S. A. Nowdeh, I. F. Davoudkhani, M. H. Moghaddam et al., "Fuzzy multi-objective placement of renewable energy sources in distribution system with objective of loss reduction and reliability improvement using a novel hybrid method," *Applied Soft Computing*, vol. 77, pp. 761–779, 2019.

[17] S. Tabatabaee, S. S. Mortazavi, and T. Niknam, "Stochastic scheduling of local distribution systems considering high penetration of plug-in electric vehicles and renewable energy sources," *Energy*, vol. 121, pp. 480–490, 2017.

[18] A. Jafar-Nowdeh, M. Babanezhad, S. Arabi-Nowdeh et al., "Meta-heuristic matrix moth–flame algorithm for optimal reconfiguration of distribution networks and placement of solar and wind renewable sources considering reliability," *Environmental Technology & Innovation*, vol. 20, article 101118, 2020.

[19] S. Alekshah, A. Rasouli, Y. Malekshah, A. Ramezani, and A. Malekshah, "Reliability-driven distribution power network dynamic reconfiguration in presence of distributed generation

by the deep reinforcement learning method," *Alexandria Engineering Journal*, vol. 61, no. 8, pp. 6541–6556, 2022.

[20] S. Sannigrahi, S. R. Ghatak, and P. Acharjee, "Multi-objective optimisation-based active distribution system planning with reconfiguration, intermittent RES, and DSTATCOM," *IET Renewable Power Generation*, vol. 13, no. 13, pp. 2418–2429, 2019.

[21] Y. Shen, G. Wang, and J. Zhu, "Resilience improvement model of distribution network based on two-stage robust optimization," *Electric Power Systems Research*, vol. 223, article 109559, 2023.

[22] H. Wang, Y. P. Fang, and E. Zio, "Resilience-oriented optimal post-disruption reconfiguration for coupled traffic-power systems," *Reliability Engineering & System Safety*, vol. 222, article 108408, 2022.

[23] H. Hou, J. Tang, Z. Zhang et al., "Resilience enhancement of distribution network under typhoon disaster based on two-stage stochastic programming," *Applied Energy*, vol. 338, article 120892, 2023.

[24] A. Khodadadi, T. Abedinzadeh, H. Alipour, and J. Pouladi, "Optimal resilient operation of smart distribution network in the presence of renewable energy resources and intelligent parking lots under uncertainties," *International Journal of Electrical Power & Energy Systems*, vol. 147, article 108814, 2023.

[25] S. Nourian and A. Kazemi, "Resilience enhancement of active distribution networks in the presence of wind turbines and energy storage systems by considering flexible loads," *Journal of Energy Storage*, vol. 48, article 104042, 2022.

[26] M. Rajabzadeh and M. Kalantar, "Enhance the resilience of distribution system against direct and indirect effects of extreme winds using battery energy storage systems," *Sustainable Cities and Society*, vol. 76, article 103486, 2022.

[27] A. Shahbazi, J. Aghaei, T. Niknam, M. Ardeshiri, A. Kavousi-Fard, and M. Shafie-khah, "Potential of mobile energy hubs for enhancing resilience of electricity distribution systems," *Electric Power Systems Research*, vol. 213, article 108749, 2022.

[28] C. Zhong, G. Li, and Z. Meng, "Beluga whale optimization: a novel nature-inspired metaheuristic algorithm," *Knowledge-Based Systems*, vol. 251, article 109215, 2022.

[29] M. Jahannoush and S. A. Nowdeh, "Optimal designing and management of a stand-alone hybrid energy system using meta-heuristic improved sine–cosine algorithm for recreational center, case study for Iran country," *Applied Soft Computing*, vol. 96, article 106611, 2020.

[30] M. Aliabadi and M. Radmehr, "Optimization of hybrid renewable energy system in radial distribution networks considering uncertainty using meta-heuristic crow search algorithm," *Applied Soft Computing*, vol. 107, article 107384, 2021.

[31] B. Cao, W. Dong, Z. Lv, Y. Gu, S. Singh, and P. Kumar, "Hybrid microgrid many-objective sizing optimization with fuzzy decision," *IEEE Transactions on Fuzzy Systems*, vol. 28, no. 11, pp. 2702–2710, 2020.

[32] I. F. Davoudkhani, A. Dejamkhooy, and S. A. Nowdeh, "A novel cloud-based framework for optimal design of stand-alone hybrid renewable energy system considering uncertainty and battery aging," *Applied Energy*, vol. 344, article 121257, 2023.

[33] Y. Qiao, F. Hu, W. Xiong, Z. Guo, X. Zhou, and Y. Li, "Multi-objective optimization of integrated energy system considering installation configuration," *Energy*, vol. 263, article 125785, 2023.

[34] M. J. H. Moghaddam, A. Kalam, J. Shi, S. A. Nowdeh, F. H. Gandoman, and A. Ahmadi, "A new model for reconfiguration and distributed generation allocation in distribution network considering power quality indices and network losses," *IEEE Systems Journal*, vol. 14, no. 3, pp. 3530–3538, 2020.

[35] A. Swarnkar, N. Gupta, and K. R. Niazi, "Adapted ant colony optimization for efficient reconfiguration of balanced and unbalanced distribution systems for loss minimization," *Swarm and Evolutionary Computation*, vol. 1, no. 3, pp. 129–137, 2011.

[36] S. Arabi-Nowdeh, S. Nasri, P. B. Saftjani et al., "Multi-criteria optimal design of hybrid clean energy system with battery storage considering off- and on-grid application," *Journal of Cleaner Production*, vol. 290, article 125808, 2021.